ΕΘΝΙΚΟ ΜΕΤΣΟΒΙΟ ΠΟΛΥΤΕΧΝΕΙΟ

ΣΧΟΛΗ ΕΦΑΡΜΟΣΜΕΝΩΝ ΜΑΘΗΜΑΤΙΚΩΝ ΚΑΙ ΦΥΣΙΚΩΝ ΕΠΙΣΤΗΜΩΝ

ΤΟΜΕΑΣ ΦΥΣΙΚΗΣ

Πειραματική και θεωρητική μελέτη της παραγωγής ισομερούς στάθμης στην αντίδραση ^{197}Au(n,2n)

ΜΕΤΑΠΤΥΧΙΑΚΗ ΕΡΓΑΣΙΑ,
ΔΠΜΣ «ΦΥΣΙΚΗ ΚΑΙ ΤΕΧΝΟΛΟΓΙΚΕΣ ΕΦΑΡΜΟΓΕΣ»

Ανδρέας Τσιγγάνης

ΑΘΗΝΑ, Σεπτέμβριος 2011

NATIONAL TECHNICAL UNIVERSITY OF ATHENS

FACULTY OF APPLIED SCIENCES

DEPARTMENT OF PHYSICS

Experimental and theoretical study of the isomeric cross section of the ^{197}Au(n,2n) reaction

M.Sc. Thesis,
Interdepartmental programme of post-graduate studies "Physics and Technological Applications"

Andreas Tsinganis

ATHENS, September 2011

Ευχαριστίες

Θα ήθελα να ευχαριστήσω τους επιβλέποντες της εργασίας αυτής, την Καθ. Ρόζα Βλαστού, τον Επ. Καθ. Μιχάλη Κόκκορη και τον Αναπ. Καθ. Κωνσταντίνο Παπαδόπουλο του Τομέα Φυσικής του Εθνικού Μετσοβίου Πολυτεχνειου που υποστήριξαν το πειραματικό και θεωρητικό σκέλος αυτής της εργασίας. Ιδιαίτερες ευχαριστίες αρμόζουν και στον Δρ. Τάσο Λαγογιάννη, ερευνητή του ΕΚΕΦΕ ‘ Δημόκριτος ’ για την ανεκτίμητη βοήθειά του στη διάρκεια των ακτινοβολήσεων. Τέλος, έπειτα από μήνες κοινής εργασίας πάνω στους θεωρητικούς υπολογισμούς που παρουσιάζονται σε αυτήν την εργασία, καθώς και στη συγγραφή της τελικής δημοσίευσης, η συνάδελφός μου Μαρία Διακάκη οπωσδήποτε κερδίζει μία πολύ σημαντική θέση σε αυτή τη σελίδα - καλύτερο από το τίποτα.

Acknowledgements

I would like to thank the supervisors of this work, Prof. Rosa Vlastou, Assistant Prof. Michael Kokkoris and Associate Prof. Costas Papadopoulos at the Department of Physics of the National Technical University of Athens who closely supported the experimental and theoretical part of this project. Special thanks are also due to Dr. Tasos Lagoyannis, researcher at the NCSR "Demokritos" for his assistance during the irradiations at the van de Graaf accelerator. Finally, after months of common work on the theoretical calculations presented in this work and in writing the final publication, my colleague Maria Diakaki definitely earns a very important spot on this page - which is better than nothing.

Περίληψη

Στην παρούσα εργασία, η ενεργός διατομή της αντίδρασης ^{197}Au(n,2n) προσδιορίστηκε πειραματικά σχετικά με την ενεργό διατομή της αντίδρασης ^{27}Al(n,α)^{24}Na σε ενέργειες προσπιπτόντων νετρονίων μεταξύ 9.0 και 10.5 MeV μέσω της τεχνικής ενεργοποίησης. Η σχεδόν μονοενεργειακή δέσμη νετρονίων παρήχθη μέσω της αντίδρασης ^{2}H(d,n)^{3}He στον επιταχυντή Tandem van de Graaff 5.5 MV του ΕΚΕΦΕ ' Δημόκριτος ' και μελετήθηκε ως προς τη συνεισφορά 'παρασιτικών' νετρονίων χρησιμοποιώντας την τεχνική πολλαπλής ενεργοποίησης και τον κώδικα αποσυνέλιξης SULSA. Οι ενεργές διατομές τροφοδότησης της δεύτερης ισομερούς κατάστασης (12^-) του ^{196}Au και το άθροισμα των ενεργών διατομών τροφοδότησης της θεμελιώδους (2^-) και πρώτης ισομερούς στάθμης (5^-) προσδιορίστηκαν ανεξάρτητα. Βοηθητικές προσομοιώσεις Monte Carlo πραγματοποιήθηκαν με τον κώδικα MCNP. Θεωρητικοί υπολογισμοί των ανωτέρω ενεργών διατομών στην ενεργειακή περιοχή 8 με 25 MeV πραγματοποιήθηκαν με τους κώδικες STAPRE-F, EMPIRE και TALYS, οι οποίοι συγκρίθηκαν και ως προς την υλοποίηση του Γενικευμένου Μοντέλου Υπερρευστού (Generalised Superfluid Model). Τα θεωρητικά αποτελέσματα συγκρίθηκαν με παλαιότερα αποτελέσματα στην ίδια περιοχή μαζών αποκαλύπτοντας την ισχυρή εξάρτηση από το ενεργειακό διάγραμμα των συμμετεχόντων πυρήνων.

Abstract

In the present work, the ^{197}Au(n,2n) reaction cross section is experimentally determined relative to the ^{27}Al(n,α)^{24}Na reaction at incident neutron energies of 9.0 to 10.5 MeV by means of the activation technique. The quasi-monoenergetic fast neutron beam was produced via the ^{2}H(d,n)^{3}He reaction at the 5.5 MV Tandem Van de Graaff accelerator at the NCSR "Demokritos" and was studied to determine the contribution of background "parasitic" neutrons using the multiple foil activation technique and the SULSA unfolding code. The cross sections for the population of the second isomeric state (12^-) of ^{196}Au and the sum of the ground (2^-) and first isomeric state (5^-) population cross sections were independently determined. Auxiliary Monte Carlo simulations were performed with the MCNP code. Theoretical calculations of the above cross sections in the 8 to 25 MeV region were carried out with the use of the STAPRE-F, EMPIRE and TALYS codes, which were also compared in their implementation of the Generalised Superfluid Model (GSM). The theoretical results are compared with previous work in the same mass region and the strong dependence on the level scheme of the nuclei involved was revealed.

Contents

Εισαγωγή

Η μελέτη ενεργών διατομών πυρηνικών αντιδράσεων είναι ένα θεμελιώδες εργαλείο της πυρηνικής φυσικής. Μέχρι σήμερα, πολλά θεωρητικά μοντέλα έχουν αναπτυχθεί για την περιγραφή των πυρηνικών μηχανισμών αντίδρασης. Η βελτίωση των θεωρητικών προβλέψεων με βάση τα μοντέλα αυτά εξαρτάται από την ύπαρξη ακριβών πειραματικών δεδομένων για την εκτίμηση των (ημι-)εμπειρικών παραμέτρων που υπεισέρχονται στους θεωρητικούς υπολογισμούς.

Η παρουσία μιας ισομερούς κατάστασης υψηλού σπιν στο θυγατρικό πυρήνα μιας αντίδρασης κατωφλίου παρέχει ένα ευαίσθητο εργαλείο για τη μελέτη των υπαρχόντων πυρηνικών μοντέλων. Η μελέτη αυτών των αντιδράσεων είναι ένα ισχυρό εργαλείο για να λάβουμε πληροφορίες για τη δομή των πυρήνων. Ειδικότερα, οι πυρήνες της μεταβατικής περιοχής από παραμορφωμένους σε σφαιρικούς πυρήνες κοντά στο κλειστό κέλυφος με Z = 82 παρουσιάζουν μια πολύ περίπλοκη δομή και για τους περισσότερους από αυτούς τους έχει αναφερθεί μία ισομερής στάθμη με υψηλό σπιν σε σχέση με το σπιν της αντίστοιχης θεμελιώδους κατάστασης. Για το ίδιο στοιχείο, η ενέργεια αυτής της ισομερούς αυξάνει με το μαζικό αριθμό.

Στο πλαίσιο αυτό, το ισότοπο ^{196}Au παρουσιάζει ένα ενδιαφέρον ζεύγος: θεμελιώδη και ισομερή στάθμη με σπιν 2^- και 12^- αντίστοιχα. Αυτή η ισομερής στάθμη έχει αναφερθεί και σε άλλα ισότοπα χρυσού (^{198}Au, ^{200}Au). Ωστόσο, μια έρευνα της βιβλιογραφίας αποκάλυψε μόνο έναν περιορισμένο αριθμό πειραματικών δεδομένων για την ενεργό διατομή της αντίδρασης ^{197}Au(n, 2n)^{196}Au^{m2}, ειδικά κοντά στην ενέργεια κατωφλίου.

Έτσι, ο σκοπός αυτής της εργασίας [1] ήταν να προσδιοριστούν πειραματικά οι ενεργές διατομές των αντιδράσεων ^{197}Au(n, 2n)^{196}Au^{m2} και ^{197}Au(n, 2n)^{196}Au^{g+m1} σε ενέργειες προσπιπτόντων νετρονίων 9.0 έως 10.5 MeV, δηλαδή κοντά στην ενέργεια κατωφλίου, με τη μέθοδο της ενεργοποίησης. Επιπλέον, θεωρητικοί υπολογισμοί στα πλαίσια του στατιστικού προτύπου έγιναν λαμβάνοντας υπ' όψιν όλα τα διαθέσιμα πειραματικά δεδομένα σε εκτεταμένο φάσμα της ενέργειας για τη μελέτη της συμβολής της κατανομής στροφορμών και των λεπτομερειών των ενεργειακών σταθμών του θυγατρικού πυρήνα στην τροφοδοσία των ισομερών σταθμών.

Στο πρώτο κεφάλαιο παρουσιάζονται οι βασικές πληροφορίες για την αντίδραση Au(n,2n), μαζί με μια επισκόπηση των προηγούμενων μετρήσεων, καθώς και μία περιγραφή της τεχνικής ενεργοποίησης. Τα πειραματικά στοιχεία της μέτρησης παρουσιάζονται στο κεφάλαιο 2 μαζί με την ανάλυση των δεδομένων και τις σχετικές διορθώσεις που εφαρμόζονται.

Στο κεφάλαιο 3 παρουσιάζονται η βασική θεωρία περί μηχανισμών πυρηνικής αντίδρασης και πυκνότητας καταστάσεων, με έμφαση στο Μοντέλο Γενικευμένου Υπερρευστού (Generalised Superfluid Model). Δίνονται επίσης πληροφορίες για τους κώδικες που χρησιμοποιήθηκαν στη θεωρητική ανάλυση. Τα αποτελέσματα των θεωρητικών υπολογισμών, καθώς και η αναλυτική διερεύνησή τους παρουσιάζονται στο κεφάλαιο 4. Τέλος, τα πειραματικά και θεωρητικά αποτελέσματα και τα συμπεράσματα παρουσιάζονται στο κεφάλαιο 5.

Εκτεταμένη περίληψη (extended Greek summary)

Η αντίδραση Au(n,2n) και η μέθοδος της ενεργοποίησης

Η αντίδραση Au(n,2n)

Η μελέτη ενεργών διατομών πυρηνικών αντιδράσεων νετρονίων μας παρέχει πληροφορίες για την κατανομή στροφορμών και την πυκνότητα πυρηνικών σταθμών του σύνθετου πυρήνα, καθώς αυτές οι ποσότητες καθορίζουν τις ενεργές διατομές για τα διάφορα κανάλια εξόδου. Αντιστοίχως, η πειραματική μέτρηση τέτοιων ενεργών διατομών ενισχύει την προσπάθεια βελτίωσης των θεωρητικών μοντέλων που περιγράφουν το πυρηνικό συνεχές.

Η αντίδραση Au(n,2n) είναι αντίδραση κατωφλίου με ενέργεια κατωφλίου E_{th}= 8.11 MeV. Η αντίδραση πραγματοποιείται μέσω δημιουργίας του σύνθετου πυρήνα ^{198}Au, ο οποίος στη συνέχεια αποδιεγείρεται στον ^{196}Au με την εκπομπή δύο νετρονίων.

Ο θυγατρικός πυρήνας ^{196}Au είναι ασταθής και αποδιεγείρεται μέσω β^+ (93%) και β^- διάσπασης (7%). Ο χρόνος ημιζωής της θεμελιώδους στάθμης είναι 6.17 ημέρες. Η αποδιέγερση συνοδεύεται από εκπομπή χαρακτηριστικών ακτίνων-γ σε ενέργειες στα 333, 356 και 426 keV.

Είναι δυνατόν, ωστόσο, ο πυρήνας ^{196}Au να βρεθεί σε διεγερμένη κατάσταση μετά την αντίδραση. Πράγματι, ο ^{196}Au έχει δύο ισομερείς στάθμες. Η πρώτη ισομερής στάθμη έχει (m1) στα 85 keV έχει χρόνο ημιζωής 8.1 s. Η δεύτερη ισομερής στάθμη (m2) στα 596 keV έχει χρόνο ημιζωής 9.7 h και αποδιεγείρεται στη θεμελιώδη στάθμη με εκπομπή ακτίνων-γ στα 148 και 188 keV.

Σκοπός αυτής της εργασίας ήταν να προσδιοριστούν πειραματικά οι ενεργές διατομές των αντιδράσεων ^{197}Au(n, 2n)^{196}Au^{m2} και ^{197}Au(n, 2n)^{196}Au^{g+m1} σε ενέργειες προσπιπτόντων νετρονίων 9.5 και 10.5 MeV, δηλαδή κοντά στην ενέργεια κατωφλίου, με τη μέθοδο της ενεργοποίησης. Οι φυσικές και χημικές του ιδιότητες, καθιστούν την κατασκευή μονοϊσοτοπικών δειγμάτων χρυσού των επιθυμητών διαστάσεων σχετικά εύκολη, ο δε χειρισμός τους δεν παρουσιάζει κάποια δυσκολία. Σχετικά με τη συγκεκριμένη μέτρηση, οι φυσικές ιδιότητες του χρυσού θέτουν ένα μόνο πειραματικό εμπόδιο: ο υψηλός συντελεστής ενδοαπορρόφησης οδηγεί σε σημαντικές απώλειες στις ανιχνευόμενες ακτίνες -γ, όπως περιγράφεται στο κεφ. 2.4.2. Λόγω του πολυ μικρού χρόνου ημιζωής, δεν ήταν δυνατή η ανεξάρτητη μελέτη της πρώτης ισομερούς στάθμης.

Η μέθοδος της ενεργοποίησης

Η μέθοδος της ενεργοποίησης συνίσταται στη μελέτη του θυγατρικού πυρήνα της αντίδρασης κατόπιν ακτινοβόλησης του στόχου. Η εφαρμογή της μεθόδου απαιτεί προφανώς ο θυγατρικός πυρήνας να είναι ασταθής ή να βρίσκεται

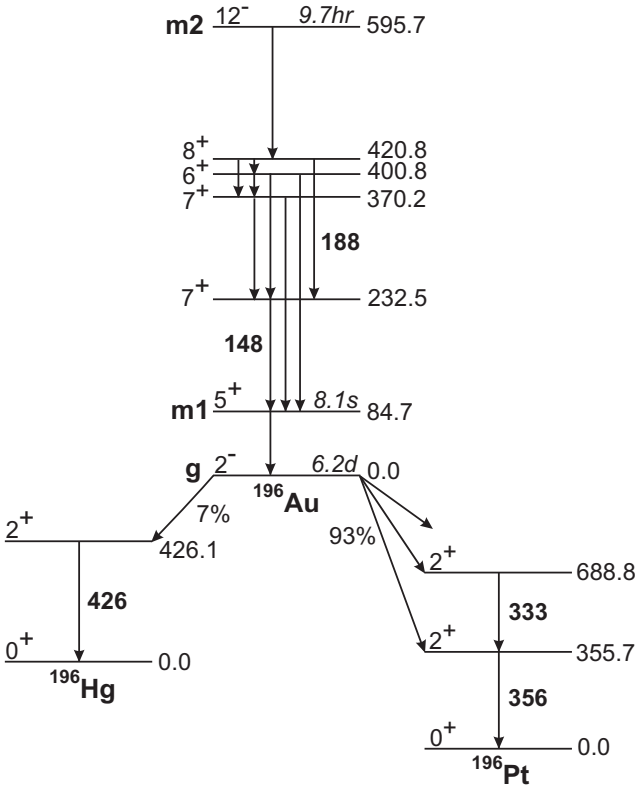

1: Απλοποιημένο διάγραμμα αποδιέγερσης των ισομερών και της θεμελιώδους στάθμης του πυρήνα ^{196}Au. Οι ενέργειες δίνονται σε keV.

σε διεγερμένη κατάσταση μετά το πέρας της ακτινοβόλησης. Μελετώντας τον αριθμό αποδιεγέρσεων που πραγματοποιούνται μετά την ακτινοβόληση, μπορούν να εκτιμηθούν ο αριθμός των αντιδράσεων που πραγματοποιήθηκαν στο στόχο και κατ΄ επέκταση η ενεργός διατομή της αντίδρασης.

Οι βασικοί πειραματικοί περιορισμοί και απαιτήσεις και τα πλεονεκτήματα της μεθόδου της ενεργοποίησης περιγράφονται αναλυτικά στο κεφ. 1.3.

Πειραματικά

Ακτινοβολήσεις σε ενέργειες 9.0 με 10.5 MeV πραγματοποιήθηκαν στον επιταχυντή 5.5 MV Tandem Van de Graaff του ΕΚΕΦΕ ‘ Δημόκριτος ’. Στη συνέχεια, ακολούθησαν μετρήσεις με χρήση ανιχνευτή Γερμανίου υψηλής καθαρότητας (HPGe) στο Εργαστήριο Πυρηνικής Φυσικής του Τομέα Φυσικής του ΕΜΠ.

Η σχεδόν μονοενεργειακή δέσμη νετρονίων παρήχθη μέσω της αντίδρασης ^{2}H(d,n)^{3}He βομβαρδίζοντας ένα στόχο δευτερίου με δέσμη δευτερονίων. Με τη διάταξη αυτή επετεύχθη ροή νετρονίων 3×10^{5}-4×10^{6} n/(cm^2·s).

Η αβεβαιότητα στην ενέργεια νετρονίων εκτιμήθηκε στα 50 keV. Η συνεισφορά ‘παρασιτικών’ νετρονίων μελετήθηκε επίσης διεξοδικά μέσω της τεχνικής πολλαπλής ακτινοβόλησης [2]. Συμπέρασμα της μελέτης αυτής ήταν ότι, αν και ο αριθμός τέτοιων νετρονίων είναι μεγάλος, η ενέργειά τους παραμένει κάτω από το κατώφλι των υπό μελέτη αντιδράσεων.

Οι ακτινοβολήσεις είχαν διάρκεια περίπου 24 ωρών. Χρησιμοποιήθηκαν στόχοι υψηλής καθαρότητας με διάμετρο 14 mm και πάχος 0.5 mm. Όμοιοι στόχοι αλουμινίου τοποθετήθηκαν πριν και μετά το στόχο χρυσού για τον προσδιορισμό της ροής νετρονίων μέσω της γνωστής ενεργού διατομής της αντίδρασης ^{27}Al(n,α)^{24}Na.

Οι στόχοι τοποθετήθηκαν κατά τρόπο που να ελαχιστοποιείται η αβεβαιότητα στην ενέργεια των νετρονίων. Οι διακυμάνσεις της δέσμης καταγράφηκαν με ανιχνευτή BF_3. Τα αντίστοιχα δεδομένα χρησιμοποιήθηκαν για την εκτίμηση του αριθμού των πυρήνων ^{196}Au που αποδιεγείρονται στην διάρκεια της ακτινοβόλησης.

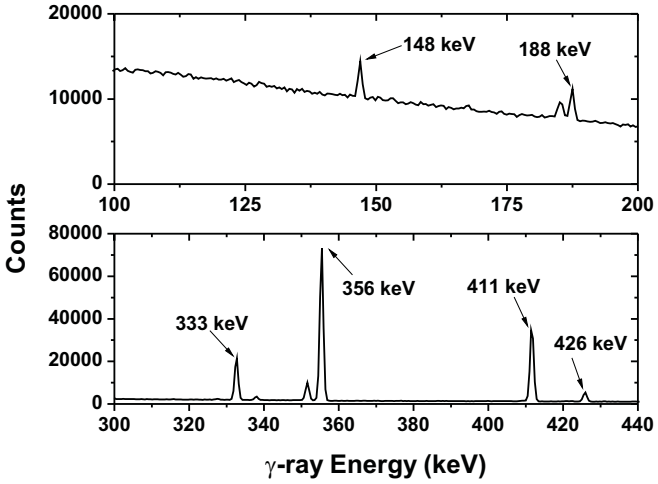

2: Πειραματικά φάσματα της αποδιέγερσης της 2ης ισομερούς στάθμης (πάνω) και της θεμελιώδους στάθμης (κάτω) του πυρήνα ^{196}Au, μετά την ακτινοβόληση στα 10.5 MeV.

1: Ιδιότητες αποδιέγερσης των θυγατρικών πυρήνων

Θυγατρικός πυρήνας	Χρόνος ημιζωής	Ενέργεια ακτίνας -γ	Ένταση (%)
^{196}Au^{g1}	6.1669±0.0006 d	333.0	22.9±0.9
		355.7	87±1
		426.1	6.6±0.1
^{196}Au^{m21}	9.7±0.1 h	147.8	43.5±0.1
		188.3	30.0±1.5
^{24}Na[2]	14.9590±0.0012 h	1368.6	100.0±0.0

[1] [3]
[2] [4]

Οι βασικές ποσότητες που αφορούν την ακτινοβόληση παρουσιάζονται στον πίνακα 2.2.

Μετρήσεις ακτίνων-γ

Μετά το πέρας της ακτινοβόλησης, ακολουθούσε μέτρηση των στοχων με χρήση ανιχνευτή Γερμανίου υψηλής καθαρότητας (HPGe). Οι στόχοι τοποθετήθηκαν σε απόσταση 10 cm από το παράθυρο του ανιχνευτή. Στην εικόνα 2 παρουσιάζονται φάσματα από τη μέτρηση για τη δεύτερη ισομερή στάθμη (επάνω) και τη θεμελιώδη στάθμη (κάτω).

Τα στοιχεία των ακτίνων-γ που χρησιμοποιήθηκαν στην ανάλυση παρουσιάζονται συγκεντρωτικά στον πίνακα 1.

Η διάρκεια των μετρήσεων ήταν περίπου 20 ώρες για τη δεύτερη ισομερή στάθμη (μέσω της ακτίνας στα 148 keV) και στη συνέχεια μέχρι 3 ώρες για τα δείγματα αλουμινίου (1369 keV). Οι μετρήσεις για τη θεμελιώδη στάθμη (356 keV) ξεκινούσαν μετά την πλήρη αποδιέγερση (μερικούς χρόνους ημιζωής) της δεύτερης ισομερούς στάθμης ($T_{1/2}$ = 9.7 h).

Ανάλυση δεδομένων

Υπολογισμός ενεργών διατομών

Για κάθε περίπτωση, η ενεργός διατομή υπολογίστηκε με βάση την παρακάτω εξίσωση:

$$\sigma = \frac{N_\gamma}{\epsilon I N_T \Phi S f D} \tag{1}$$

όπου N_γ ο αριθμός γεγονότων της αντίστοιχης φωτοκορυφής. Ο παράγοντας ϵ εκφράζει την απόδοση του ανιχνευτή, I είναι η ένταση της ακτίνας -γ, N_T ο αριθμός των πυρήνων του στόχου και S ο συντελεστής ενδοαπορρόφησης. Οι αποδιεγέρσεις που πραγματοποιούνται κατά τη διάρκεια της ακτινοβόλησης και πριν την έναρξη της μέτρησης λαμβάνονται υπ΄ όψιν με τον διορθωτικό παράγοντα f που δίνεται ως:

$$f = \frac{\int_0^{t_b} e^{-\lambda t} F(t)\, dt}{\int_0^{t_b} F(t)\, dt} e^{-\lambda t_b}, \tag{2}$$

όπου t_b ο χρόνος ακτινοβόλησης και $F(t)$ η ροή νετρονίων σε αυθαίρετες μονάδες όπως δίνονται από τον ανιχνευτή BF_3, ενώ ο διορθωτικός παράγοντας D αφορά το διάστημα ανάμεσα στο τέλος της ακτινοβόλησης και το τέλος της μέτρησης και δίνεται ως:

$$D = (1 - e^{-\lambda t_m}) e^{-\lambda t_w}, \tag{3}$$

όπου t_w και t_m είναι ο χρόνος ανάμεσα στο τέλος της ακτινοβόλησης και τη μέτρηση και ο χρόνος της μέτρησης αντίστοιχα.

Η συνολική ροή νετρονίων Φ υπολογίστηκε βάση της ενεργού διατομής της αντίδρασης $^{27}\mathrm{Al(n,\alpha)}^{24}\mathrm{Na}$ που είναι διαθέσιμη στη βιβλιογραφία [5] και υπολογίζοντας τη μέση τιμή από τους δύο στόχους αλουμινίου.

Οι αβεβαιότητες όλων των παραγόντων που υπεισέρχονται στον υπολογισμό των ενεργών διατομών παρουσιάζονται αναλυτικά στον πίνακα 2.4.

Διορθώσεις ενδοαπορρόφησης

Δεδομένης της σχετικά χαμηλής ενέργειας των ακτίνων-γ και του υψηλού συντελεστή απορρόφησης του χρυσού ήταν απαραίτητη η εκτιμηση της ενδοαπορρόφησης στο δείγμα. Προσομοιώσεις Monte-Carlo με χρήση του κώδικα MCNP [6] έδειξαν ότι περίπου 55% των ακτίνων στα 148 keV και 12% των ακτίνων στα 356 keV χάνονται λόγω ενδοαπορρόφησης σε ένα δείγμα χρυσού πάχους 0.5 mm. Η ενδοαπορρόφηση της ακτίνας -γ του αλουμινίου στα 1369 keV βρέθηκε να είναι μικρότερη του 0.5%.

Αποτελέσματα

Τα νέα πειραματικά δεδομένα φαίνονται στις εικόνες 3 και 4 μαζί με παλαιότερες μετρήσεις.

Πυρηνικές αντιδράσεις και πρότυπα πυκνότητας πυρηνικών σταθμών

Μηχανισμοί πυρηνικής αντίδρασης

Ανάλογα με τον τρόπο που πραγματοποιείται η αλληλεπίδραση του βλήματος με τον πυρήνα-στόχο, οι πυρηνικές αντιδράσεις μπορούν να ταξινομηθούν σε τρεις κατηγορίες: τις άμεσες, τις αντιδράσεις προϊσορροπίας και τις αντιδράσεις σύνθετου πυρήνα.

Για να πραγματοποιηθεί μία *άμεση αντίδραση*, το βλήμα πρέπει να έχει τέτοιο μήκος κύματος ώστε να μπορεί να αλληλεπιδράσει με μεμονωμένα νουκλεόνια του στόχου ($\lambda \approx$1fm). Έτσι, η πιθανότητα πραγματοποίησης άμεσης αντίδρασης αυξάνεται με την ενέργεια του βλήματος. Η εκπομπή των προϊόντων της αντίδρασης γίνεται σε πολύ

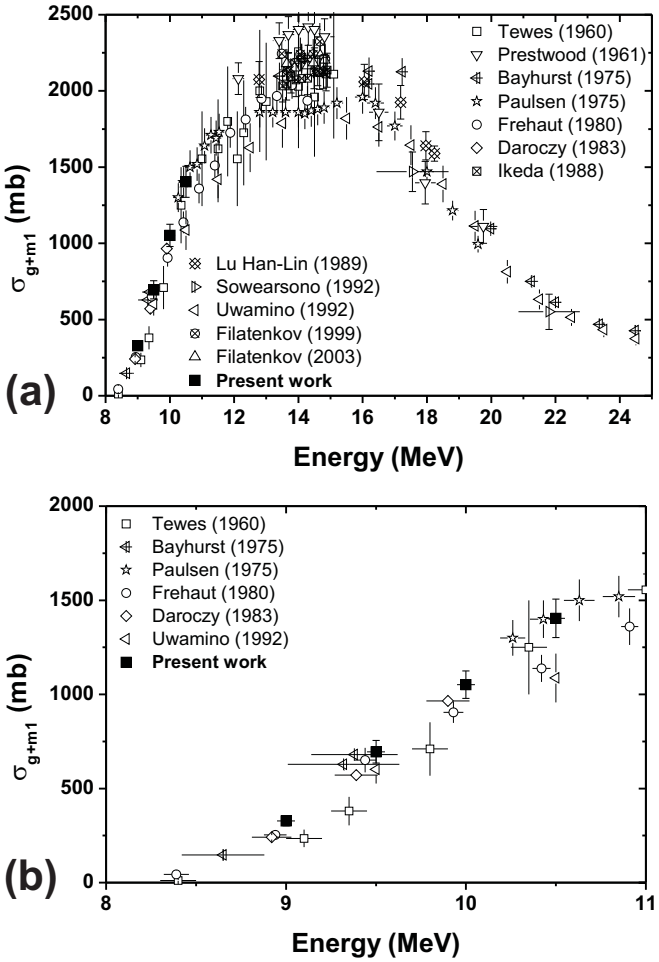

3: Πειραματικά αποτελέσματα της παρούσης εργασίας και παλαιότερες μετρήσεις της ενεργού διατομής δημιουργίας της θεμελιώδους και πρώτης ισομερούς στάθμης του πυρήνα ^{196}Au (g+m1) μεταξύ 8-25 MeV (a) και 8.5-11 MeV (b).

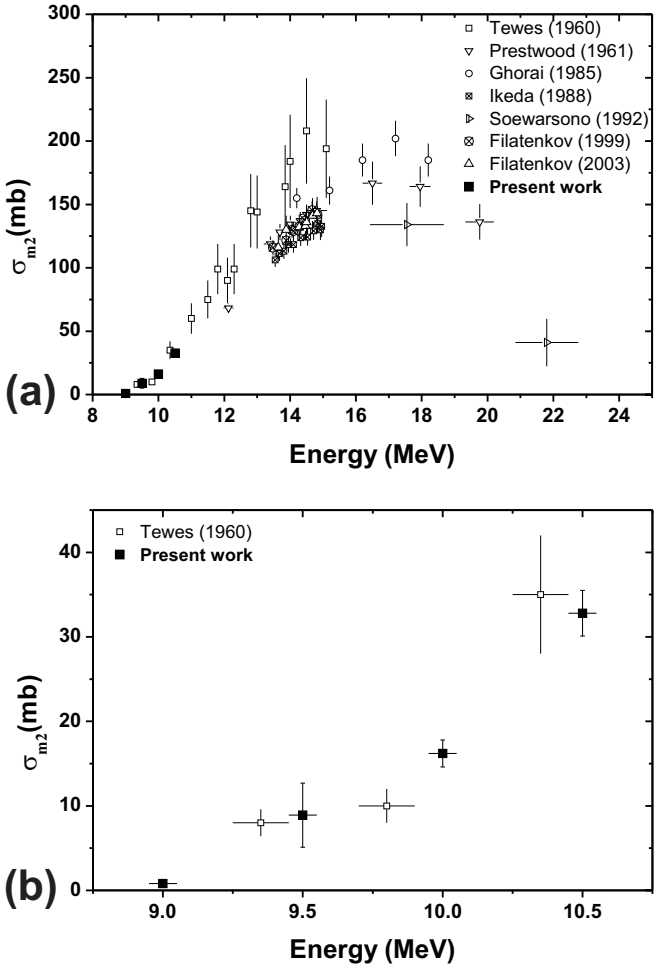

4: Πειραματικά αποτελέσματα της παρούσης εργασίας και παλαιότερες μετρήσεις της ενεργού διατομής δημιουργίας της δεύτερης ισομερούς στάθμης του πυρήνα ^{196}Au (m2) μεταξύ 8-25 MeV (a) και 8.5-11 MeV (b).

σύντομους χρόνους (10^{-22}s) και κατά προτίμηση κοντά στη φορά του βλήματος. Οι (αν)ελαστικές σκεδάσεις και οι αντιδράσεις (d,p), (p,d) είναι χαρακτηριστικές περιπτώσεις άμεσων αντιδράσεων.

Οι άμεσες αντιδράσεις περιγράφονται με το λεγόμενο 'οπτικό μοντέλο', όπου η αντίδραση περιγράφεται ως αλληλεπίδραση του βλήματος με ένα μιγαδικό δυναμικό $V(r) = -V - iW$, κατ' αναλογία με τη διαδικασία σκέδασης/απορρόφησης φωτός από μία μελανή σφαίρα.

Εφόσον το βλήμα έχει το χρόνο να αλληλεπιδράσει με μερικά από τα νουκλεόνια του στόχου τότε αρχίζει να δημιουργείται ένα σύνθετο σύστημα καθώς η ενέργεια του βλήματος μοιράζεται στα γειτονικά νουκλεόνια. Αν κατά τη διάρκεια αυτής της διαδικασίας ένα νουκλεόνιο αποκτήσει αρκετή ενέργεια ώστε να εκπεμφθεί (προτού επιτευχθεί ισορροπία στο σύστημα), τότε μιλάμε για *αντίδραση προϊσορροπίας*.

Αντιδράσεις σύνθετου πυρήνα

Ο μηχανισμός σύνθετου πυρήνα βασίζεται στην υπόθεση ότι η αντίδραση πραγματοποιείται σε δύο στάδια. Αρχικά, το βλήμα εισέρχεται και συλλαμβάνεται από τον πυρήνα με αποτέλεσμα τη δημιουργία ενός σύνθετου συστήματος. Στη συνέχεια, μέσω ενός μεγάλου αριθμού αλληλεπιδράσεων νουκλεονίου-νουκλεονίου η ενέργεια του βλήματος μοιράζεται ανάμεσα στα νουκλεόνια του σύνθετου πυρήνα και επιτυγχάνεται ισορροπία. Στατιστικές διακυμάνσεις μπορούν να οδηγήσουν ένα νουκλεόνιο που βρίσκεται κοντά στην επιφάνεια του πυρήνα να αποκτήσει επαρκή ενέργεια ώστε να υπερνικήσει το πυρηνικό δυναμικό, κατ' αναλογία με την εξάτμιση ενός υγρού. Η διαδικασία αυτή προφανώς ευνοεί την εκπομπή νετρονίων που δεν υφίστανται την επίδραση του δυναμικού Coulomb. Στη συνέχεια, ο σύνθετος πυρήνας αποδιεγείρεται είτε με την εκπομπή περαιτέρω σωματιδίων αν υπάρχει επαρκής ενέργεια ή μέσω αποδιέγερσης -γ.

Το βασικό σημείο είναι ότι η αποδιέγερση του σύνθετου πυρήνα είναι ανεξάρτητη από τον τρόπο σχηματισμού του (το κανάλι εισόδου), αλλά εξαρτάται μόνο από την ενέργεια, στροφορμή και ομοτιμία που έχει αποκτήσει.

Πρέπει να σημειωθεί ότι όλοι οι μηχανισμοί συνεισφέρουν σε διαφορετικό βαθμό σε μία αντίδραση. Αυτό εξαρτάται από διάφορους παράγοντες, όπως η ενέργεια και το φορτίο του βλήματος, οι μάζες του βλήματος και του στόχου και η δομή του σύνθετου συστήματος (ενεργειακές στάθμες, ενέργεια διέγερσης, κατανομή στροφορμών κτλ.).

Οι θεωρητικοί υπολογισμοί της ενεργού διατομής της αντίδρασης ^{197}Au(n,2n) πραγματοποιήθηκαν σε ενέργειες 8 - 25 MeV λαμβάνοντας υπ' όψιν το μηχανισμό σύνθετου πυρήνα, καθώς και συνεισφορές προϊσορροπίας στα πλαίσια της θεωρίας Hauser-Feshbach [7] και του μοντέλου εξιτονίων [8] αντίστοιχα.

Πυκνότητα πυρηνικών σταθμών

Διάφορα μοντέλα έχουν προταθεί για την περιγραφή της πυκνότητας καταστάσεων στο πυρηνικό συνεχές μέσω παραμέτρων των οποίων η τιμή εκτιμάται μέσω σύγκρισης με πειραματικά δεδομένα. Τέτοια είναι το Μοντέλο Αερίου Fermi (Fermi Gas Model - FGM), το Μοντέλο Σταθερής Θερμοκρασίας (Constant Temperature Model - CTM) και το Γενικευμένο Μοντέλου Υπερρευστού (Generalised Superfluid Model - GSM).

Σε κάθε περίπτωση γίνεται η υπόθεση ότι η εξάρτηση της πυκνότητας καταστάσεων από την ενέργεια, τη στροφορμή και την ομοτιμία μπορούν να μελετηθούν ανεξάρτητα έτσι ώστε $\rho(U, J, \pi) = \rho(U)f(J)\rho(\pi)$.

Το Γενικευμένο Πρότυπο Υπερρευστού (Generalised Superfluid Model)

Στα πλαίσια των υπολογισμών για την αντίδραση ^{197}Au(n,2n) η πυκνότητα καταστάσεων περιγράφηκε στα πλαίσια του GSM στην φαινομενολογική του μορφή όπως αναπτύχθηκε από τον Ignatyuk [9, 10]. Βασιζόμενο στον απλούστερο φορμαλισμό προηγούμενων μοντέλων, το GSM λαμβάνει υπ' όψιν επιπλέον φαινόμενα. Έχει χρησιμοποιηθεί με επιτυχία στο παρελθόν για υπολογισμούς στο ^{191}Ir [11].

Στα πλαίσια του GSM, οι ποσότητες που περιγράφουν το διεγερμένο πυρήνα δε θεωρούνται σταθερές, αλλά μεταβάλλονται με την ενέργεια διέγερσης. Η δε συμπεριφορά του συστήματος περιγράφεται από διαφορετικές εξισώσεις σε δύο ενεργειακές περιοχές που καθορίζονται από μία 'κρίσιμη' ενέργεια U_{cr}.

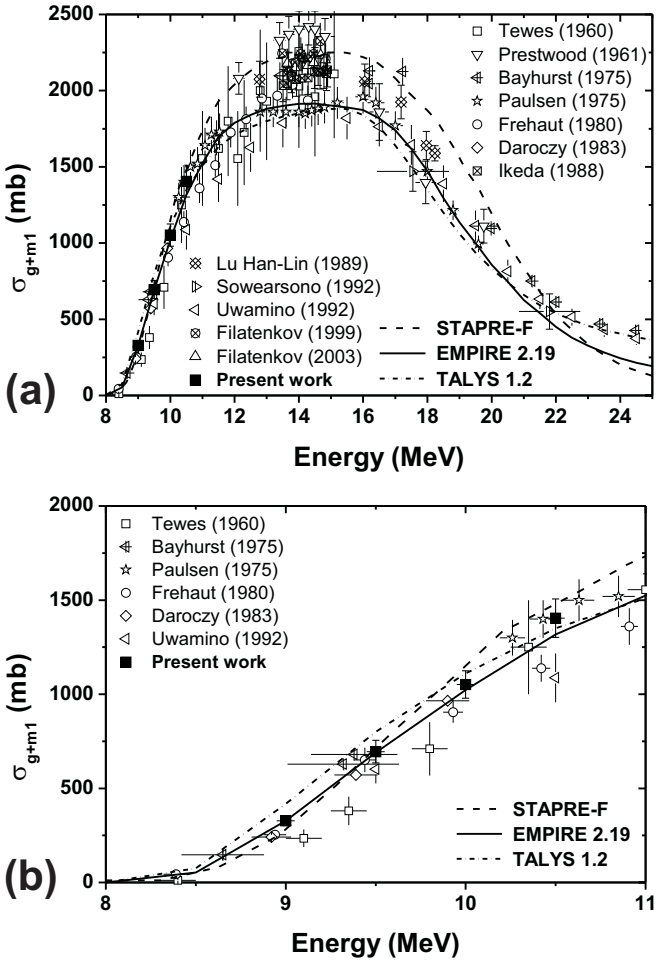

5: Θεωρητικοί υπολογισμοί και πειραματικά αποτελέσματα της ενεργού διατομής δημιουργίας της θεμελιώδους και πρώτης ισομερούς στάθμης του πυρήνα ^{196}Au (g+m1) μεταξύ 8-25 MeV (a) και 8.5-11 MeV (b)

Κώδικες πυρηνικών αντιδράσεων

Οι θεωρητικοί υπολογισμοί πραγματοποιήθηκαν με χρήση τριών κωδικών: το STAPRE-F [12], το EMPIRE 2.19 [13] και το TALYS-1.2 [14]. Και στις τρεις περιπτώσεις, η επιλογή των συντελεστών διέλευσης, της συνεισφοράς προϊσορροπίας και της πυκνότητας καταστάσεων έγιναν κατά τρόπο ώστε να γίνει σύγκριση της υλοποίησης του GSM από τους τρεις κώδικες. Λεπτομέρειες για τη δομή και λειτουργία των κωδίκων δίνονται στο κεφ. 3.3.

Θεωρητικά αποτελέσματα και διερεύνηση

Αποτελέσματα

Τα αποτελέσματα των θεωρητικών υπολογισμών για τις ενεργές διατομές σ_{g+m1} και σ_{m2}, μαζί με τα πειραματικά δεδομένα φαίνονται στις εικόνες 5 και 6 αντίστοιχα.

Όπως φαίνεται στην εικόνα 5, και οι τρεις κώδικες αναπαράγουν αρκετά καλά την ενεργό διατομή σ_{g+m1}. Στην περιοχή 12-16 MeV οι μεγάλες διαφορές ανάμεσα στα διαθέσιμα πειραματικά δεδομένα δεν επιτρέπουν να σχηματιστεί ξεκάθαρη εικόνα για την ποιότητα των θεωρητικών υπολογισμών.

Σχετικά με την ενεργό διατομή σ_{m2}, τα αποτελέσματα των STAPRE-F και EMPIRE φαίνεται να υποεκτιμούν την ενεργό διατομή σε ενέργειες μέχρι 13 MeV ενώ την υπερεκτιμούν κατά περίπου 100 mb στις υψηλές ενέργειες.

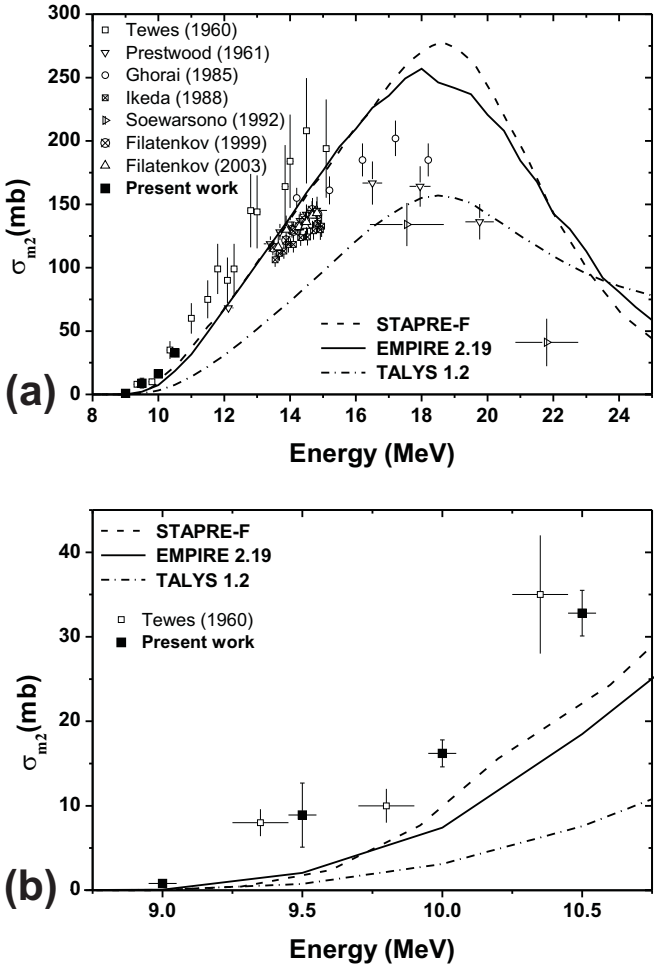

6: Θεωρητικοί υπολογισμοί και πειραματικά αποτελέσματα της ενεργού διατομής δημιουργίας της δεύτερης ισομερούς στάθμης του πυρήνα ^{196}Au (m2) μεταξύ 8-25 MeV (a) και 8.5-11 MeV (b).

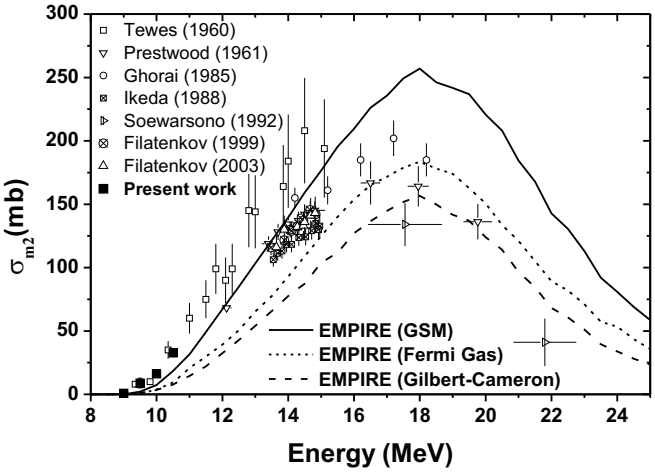

7: Θεωρητικοί υπολογισμοί της σ_{m2} με χρήση των προτύπων του αερίου Fermi και Gilbert-Cameron, σε σύγκριση με τα αποτελέσματα με χρήση του GSM.

Τα αποτελέσματα του TALYS υποεκτιμούν την ενεργό διατομή σε όλη την υπό μελέτη ενεργειακή περιοχή, μία συμπεριφορά που καταγράφηκε και στην εργασία [15]. Επιπλέον, το μέγιστο της ενεργού διατομής δίνεται και από τους τρεις κώδικες περίπου στα 18 MeV, δηλαδή περίπου 2 MeV υψηλότερα από ό,τι φαίνεται στα πειραματικά δεδομένα. Το αποτέλεσμα αυτό διερευνήθηκε διεξοδικά.

Συνολικά, και οι τρεις κώδικες ακολουθούν τη γενική συμπεριφορά των πειραματικών δεδομένων.

Περαιτέρω διερεύνηση

Βάσει των προηγούμενων παρατηρήσεων έγιναν διάφορες δοκιμές για την καλύτερη κατανόηση των αποτελεσμάτων.

Η επιρροή των επί μέρους θεωρητικών παραμέτρων στο αποτέλεσμα διερευνήθηκαν με το STAPRE-F που επιτρέπει τη μεταβολή τους 'με το χέρι'. Μεταβάλλοντας τις διάφορες παραμέτρους εντός των πειραματικών τους αβεβαιοτήτων αλλά και ακολουθώντας διαφορετικές συστηματικές. Επίσης έγιναν αλλαγές στη συνεισφορά του μηχανισμού προϊσορροπίας και στις υποθέσεις για το σχήμα και τη συμμετρία ων ισοτόπων του χρυσού, χωρίς ωστόσο σε καμία περίπτωση η διαφορές να υπερβαίνουν το 10%, ενώ η συμπεριφορά της ενεργού διατομής παρέμεινε η ίδια [16].

Προκειμένου να διαπιστωθεί κατά πόσον η παρατηρούμενη συμπεριφορά οφείλεται σε ιδιοτροπία του GSM, ο κώδικας EMPIRE χρησιμοποιήθηκε για να επαναληφθούν οι υπολογισμοί στα πλαίσια διαφορετικών προτύπων πυρηνικών πυκνοτήτων. Η υλοποίηση αυτών των δοκιμών είναι πολύ εύκολη στο EMPIRE. Χρησιμοποιήθηκαν το Back Shifted Fermi Gas Model [17] και το μοντέλο Gilbert-Cameron [18]. Τα αποτελέσματα (εικ. 7) δείχνουν ότι η επιλογή του μοντέλου πυρηνικών πυκνοτήτων δεν επηρεάζει τη συμπεριφορά της υπολογιζόμενης ενεργού διατομής σ_{m2}.

Σε παλαιότερες μελέτες στην ίδια περιοχή [11, 19–21] διεφάνη η ανάγκη μείωσης της ροπής αδρανείας των πυρήνων για την καλύτερη αναπαραγωγή των ενεργών διατομών. Στην προκειμένη περίπτωση, οι υπολογισμοί επαναλήφθηκαν με τιμές της ροπής αδρανείας μειωμένες κατά 25 και 50% χρησιμοποιώντας τους κώδικες STAPRE-F και EMPIRE. Η μείωση της ροπής αδρανείας προκαλεί σημαντική μείωση της ενεργού διατομής σ_{m2} αλλά δε βελτιώνει αισθητά τη συμφωνία με τα πειραματικά δεδομένα, όπως φαίνεται στην εικόνα 8

Με βάση τα παραπάνω αποτελέσματα, μελετήθηκε η υπόθεση ελλείψεων στα ενεργειακά διαγράμματα, ειδικά των πυρήνων ^{196}Au και ^{195}Au. Η ύπαρξη σταθμών υψηλού σπιν πάνω από τη δεύτερη ισομερή στάθμη θα οδηγούσε στην τροφοδοσία της μέσω αποδιεγέρσεων-γ. Σε παρόμοια περίπτωση, η ύπαρξη περιστροφικών σταθμών πάνω από την ισομερή στάθμη 16^+ του ^{178}Hf προτάθηκε [22] για την καλύτερη αναπαραγωγή της ενεργού διατομής ^{179}Hf(n,2n) στα πλαίσια της θεωρίας Hauser-Feshbach. Η ύπαρξη των σταθμών αυτών επιβεβαιώθηκε πειραματικά αργότερα [23].

Το ενεργειακό διάγραμμα του ^{195}Au επίσης αναμένεται να παίζει σημαντικό ρόλο σε ενέργειες άνω των 16 MeV όπου ανοίγει το κανάλι (n,3n) και παρατηρούνται οι μεγαλύτερες αποκλίσεις των θεωρητικών υπολογισμών. Συγκρίνοντας

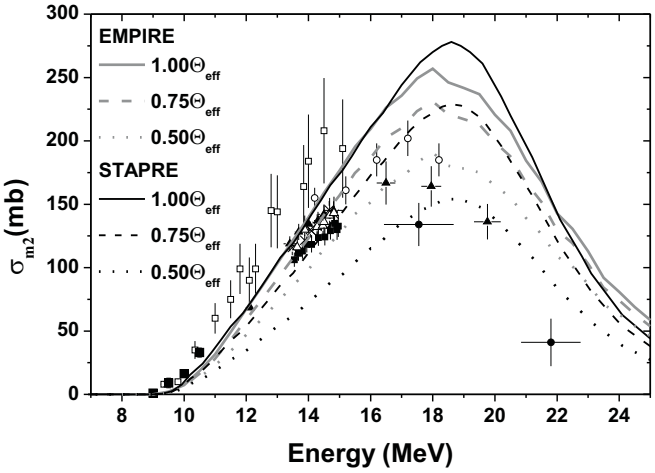

8: Θεωρητικοί υπολογισμοί της σ_{m2} με χρήση τιμών της ροπής αδράνειας μειωμένων κατά 25 και 50%.

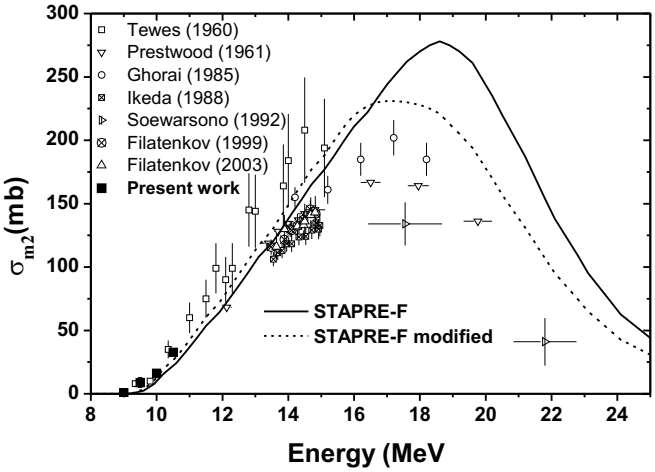

9: Θεωρητικοί υπολογισμοί της σ_{m2} με χρήση τροποποιημένου ενεργειακού διαγράμματος για τους ^{196}Au και ^{195}Au εισάγοντας υποθετικές στάθμες υψηλού σπιν.

με τα ενεργειακά διαγράμματα γειτονικών πυρήνων [24–26] εικάζεται πιθανή απουσία περιστροφικών σταθμών στις καταγεγραμμένες στάθμες του ^{195}Au. Η εισαγωγή τέτοιων σταθμών θα οδηγούσε στη μείωση της θεωρητικής ενεργού διατομής σ_{m2} άνω των 16 MeV.

Παρ΄ ότι οι υποθέσεις αυτές φαίνονται φυσικά ρεαλιστικές, δεν υπάρχει δυστυχώς η δυνατότητα εισαγωγής διακριτών σταθμών στο συνεχές με χρήση των διαθέσιμων κωδίκων ώστε να διερευνηθεί αυτή η υπόθεση.

Η μοναδική δοκιμή που ήταν δυνατόν να πραγματοποιηθεί ήταν η εισαγωγή μερικών διακριτών σταθμών υψηλού σπιν ($12^{\pm}$,$13^{\pm}$,$14^{\pm}$) στο διακριτό πάνω από την ισομερή στάθμη 12^{-} με χρήση του κώδικα STAPRE-F. Κατά τον τρόπο αυτό, ενισχύεται η τροφοδοσία της ισομερούς στάθμης και κατά συνέπεια και η ενεργός διατομή σ_{m2}, χωρίς όμως να επηρεάζεται σημαντικά η σ_{g+m1}. Γενικώς οι υπολογιζόμενες ενεργές διατομές μεταβάλλονται προς τη σωστή κατεύθυνση (εικ. 9).

Συμπεράσματα

Η πειραματική αναζήτηση περιστροφικών σταθμών υψηλού σπιν που φαίνεται να απουσιάζουν από τα διαθέσιμα ενεργειακά διαγράμματα των πυρήνων ^{196}Au και ^{195}Au καθώς και η πειραματική και θεωρητική μελέτη ισομερών σταθμών υψηλού σπιν σε αυτήν την περιοχή μαζών θα παρουσίαζαν μεγάλο ενδιαφέρον. Από πλευράς λογισμικού, η δυνατότητα εισαγωγής διακριτών σταθμών στο συνεχές θα ωφελούσε σημαντικά την ακρίβεια και το εύρος εφαρμογής των υπαρχόντων κωδικών.

Introduction

The study of nuclear reaction cross sections is a fundamental tool of nuclear physics. To this day, numerous theoretical models have been developed for the description of nuclear reaction mechanisms. The improvement of theoretical predictions based on these models relies on the existence of accurate experimental data to estimate the (semi-)empirical parameters involved in the theoretical calculations.

The presence of a high spin isomeric state in the residual nucleus of a neutron threshold reaction provides a sensitive test for existing nuclear models. The study of such reactions is a powerful tool for getting information on the structure of nuclei. In particular, the nuclei of the transitional region from well deformed to spherical nuclei near the Z=82 shell closure (Os-Pb region) present a very complex structure (γ-softening, triaxiality, shape coexistence) and for most of them an isomer with a high spin value with respect to the spin of the corresponding ground state has been reported. For the same element the energy of this isomer increases with increasing mass number A. Its existence is attributed to the coupling of high spin intruder states, and the systematic study of the excitation function of the formation of both the ground and the high spin isomeric state on the basis of a statistical model provides information on the energy and spin distribution of the level density of the nuclei involved [27] and on the changes in the structure of the low-lying excited states of the corresponding nuclei.

In this context the ^{196}Au isotope presents an interesting isomeric pair: ground and isomeric states with spin values of 2^- and 12^- respectively (Fig. 1.1). This 12^- isomer has been reported for other even A Au isotopes (^{198}Au, ^{200}Au) [28]. However, a survey of the literature revealed only a limited number of experimental data for the cross section of the ^{197}Au(n,2n)^{196}Au^{m2} reaction, especially near its threshold, where only one unpublished dataset was found.

Thus, the purpose of this work [1] was to experimentally determine the ^{197}Au(n,2n)^{196}Au^{m2} and the ^{197}Au(n,2n)^{196}Au^{g+m1} reaction cross sections in the incident neutron energy range between 9 and 10.5 MeV, i.e. close to the threshold, by means of the activation technique. Additionally, theoretical statistical model calculations were performed and compared to all available experimental data over an extended energy range to study the contribution of the spin distribution and the details of the level scheme of the residual nucleus to the formation of the isomeric state.

In chapter one, the essential information on the Au(n,2n) reaction is laid out, along with an overview of previous measurements and a description of the activation technique. The experimental aspects of the measurement, the data analysis and relevant corrections applied are described in chapter two.

A presentation of the underlying theory of nuclear reaction mechanisms and nuclear level densities, as well as details of the nuclear reaction codes used for the theoretical calculations are presented in chapter three. Chapter four includes the results provided by these codes, their comparison and detailed investigation. Finally, experimental and theoretical results and conclusions are presented in chapter five.

Part I

Experimental study of the Au(n,2n) reaction

Chapter 1

The Au(n,2n) reaction and the activation method

1.1 The Au(n,2n) reaction

The study of neutron threshold reactions can provide information on the spin distribution and level density of the compound nucleus since these properties, along with the discrete level spins and energies of the daughter nuclei, will define the cross sections for each exit channel. Conversely, the experimental measurement of these cross sections can assist in the evaluation and fine-tuning of theoretical nuclear models used to describe the nuclear continuum.

Only one stable gold isotope exists in nature, namely ^{197}Au. Other isotopes, ranging from ^{169}Au to ^{205}Au have been artificially produced and only ^{195}Au has a relatively long half-life of 186 days. Natural gold, therefore, consists only of ^{197}Au. Furthermore, it is the most ductile metal and, with few exceptions, chemically inert. These properties make the creation of pure gold samples of the desired size and thickness relatively easy. The handling and storage of the samples also present no particular difficulties. Concerning the present measurement, the physical properties of gold pose only one experimental difficulty: the high mass attenuation coefficient, leading to a significant loss of the decay γ-rays, as will be described in section 2.4.2.

The Au(n,2n) reaction is a threshold reaction, with E_{th}= 8.11 MeV. The reaction proceeds through the formation of the compound nucleus ^{198}Au. For these incident neutron energies, the ^{198}Au nucleus is formed in an excited state of about 15.5 - 17 MeV. It then decays to ^{196}Au with the emission of two neutrons.

The daughter nucleus ^{196}Au is unstable and decays by β^+ (93%) and β^- decay (7%) to the stable isotopes ^{196}Pt and ^{196}Hg correspondingly. The half-life for the ground state of ^{196}Au is 6.17 d. Characteristic γ-rays from this decay are emitted are 333, 356 and 426 keV.

It is possible, however, for ^{196}Au to be found in an excited state after the reaction. Indeed, ^{196}Au has two isomeric states. Isomeric states are nuclear states whose decay half-life is much longer than what is typical for γ-decays. This is governed by the energy and spin difference of the initial and final states with typical values of a few hundred keV for the energy difference and ΔJ=3,4,... mediated by electrical multipoles. Isomeric half-lives can therefore range from ms to years, compared to typical decay times between 10^{-17} and 10^{-10} s.

The first isomeric state of ^{196}Au (m1) at 85 keV has a half-life of 8.1 s with ΔJ=3 (E3) relative to the 2^- ground state. The second isomeric state (m2) at 596 keV has a half-life of 9.7 h and decays through the 421keV state (ΔJ=4, M4) to the ground state emitting 148 and 188 keV γ-rays.

The purpose of the measurement was to study the reaction cross section for the formation of the ground and second isomeric states of ^{196}Au at incident neutron energies between 9.0 and 10.5 MeV, very close to the reaction threshold. It was not possible to study the first isomeric state independently due to the short half-life.

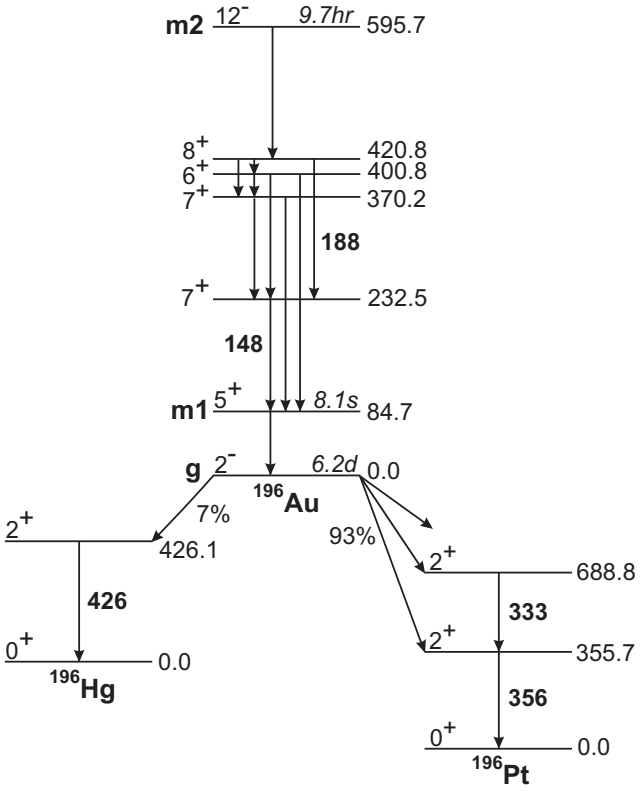

Figure 1.1: Simplified decay scheme of the isomeric and ground states of the residual nucleus ^{196}Au. All energies are given in keV.

1.2 Literature survey

Several measurements of the ground state cross section are present in existing literature, particularly at energies around 14MeV. These datasets are generally in agreement within 20% up to 12MeV, with the most notable discrepancies occurring in the 12-17MeV region (fig. 1.2).

Literature on the second isomeric state is much more sparse. Only one previous dataset exists in the energy region from threshold to 13 MeV, contained in an unpublished report [29]. It has been impossible to obtain relevant information on the particular experiment, such as beam parameters, flux, irradiation intervals and the detector(s) used for the off-line measurements. A dataset of evaluated data in this region can additionally be found in [30], also an unpublished report (fig. 1.3).

1.3 The activation method

The activation method consists of the off-line study of the daughter nucleus of a reaction, rather than the on-line detection of the outgoing particle(s). The application of this technique requires the daughter nucleus to be unstable or in an excited state. By studying its decay after the end of the irradiation, the number of reactions taking place in the sample and, consequently, the reaction cross section, can be estimated.

The main experimental limitations and advantages of the activation method can be summarised as follows.

The half-life of the daughter nucleus should not be much shorter than the time that elapses between the end of the irradiation and completion of the measurement. This is the reason why the 8.1 s isomer of ^{196}Au cannot be studied independently with the available setup. This difficulty could be overcome by means of a pneumatic rabbit system, but again not for half-lives of less than a few seconds. Furthermore, the half-life should not be so long that it is not possible to induce sufficiently high activity in the sample to obtain adequate statistics

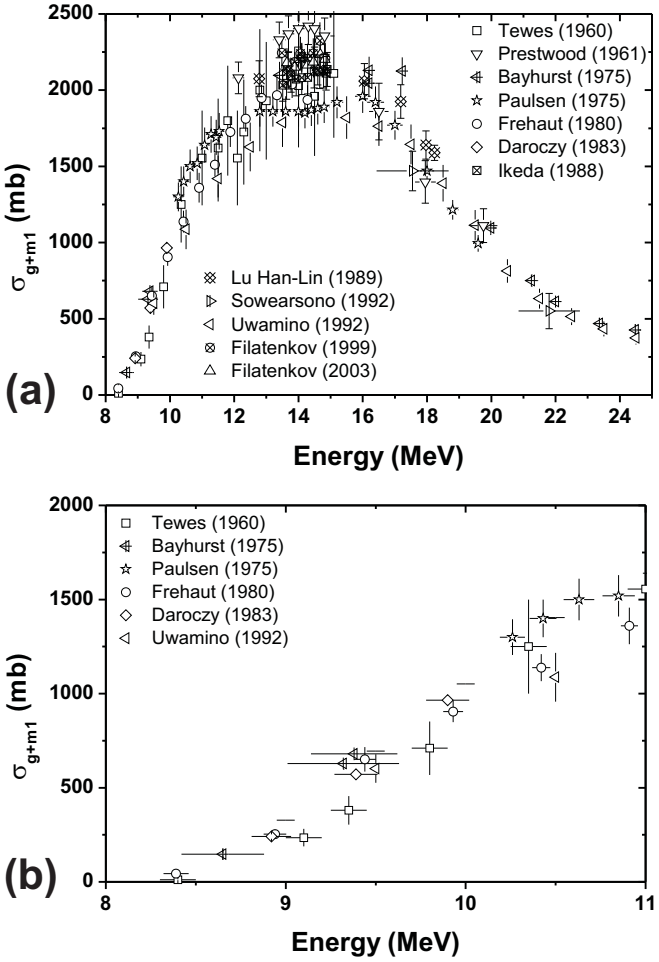

Figure 1.2: Previous experimental data for the population of the ground and first isomeric state of ^{196}Au (g+m1) between 8-25 MeV (a) and 8.5-11 MeV (b). Several datasets around 14 MeV have been omitted for clarity.

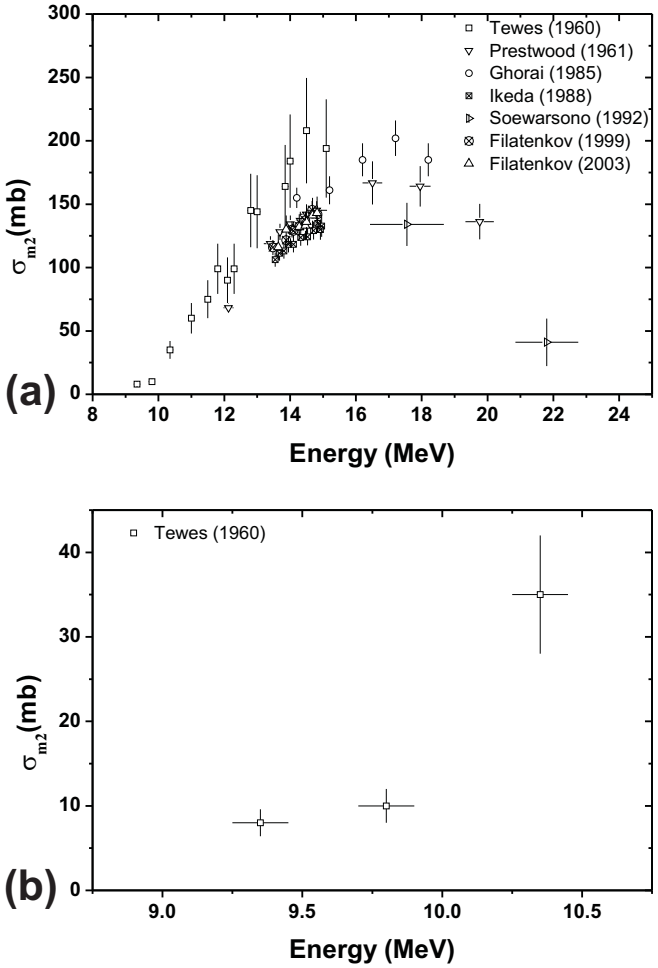

Figure 1.3: Previous experimental data for the population of the second isomeric state of ^{196}Au (m2) between 8-25 MeV (a) and 8.5-11 MeV (b).

following an irradiation of reasonable duration.

The occurrence of β^+ decays in the sample can lead to an increased Compton background below 511 keV in the acquired spectrum. This can pose a problem when the γ-rays of interest lie in this region, as is the case with this measurement.

The activation method cannot be applied when more than one isotope present in the sample can lead to the same daughter nucleus, since it would not be possible to isolate each contribution. Furthermore, the daughter nucleus should remain within the sample (e.g. it should not be a gas under normal laboratory conditions). Neither of these aspects is relevant to the case of ^{197}Au.

An activation measurement cannot be reliable if secondary reactions take place in the sample at considerable rates. We refer by this term to reactions caused by products of the main reactions or by reaction of the beam particles with the main reaction products. The magnitude of this contribution is governed mainly by the cross section ratio of the main and the secondary reactions. For high energy neutron reactions it is generally negligible, since the relevant cross sections are quite small and the number of secondary particles produced is very limited compared to the number of beam particles and target nuclei.

Finally, it is obvious that no information on the differential reaction cross section can be obtained with an activation measurement, since the daughter nucleus retains no memory of the incoming particle direction.

Among the main advantages presented by the activation method we can highlight the following. Off-line measurements generally require simpler detection systems. Furthermore, detectors used on-line are more susceptible to radiation damage due to the high flux of beam and secondary particles. The presence of these particles will also induce a significant background in the measurement which is not present in an off-line measurement and can increase the sensitivity of the activation method to detect even trace elements in the sample. To the extent that the presence of more samples does not significantly alter the beam characteristics, several samples can be irradiated at once for subsequent study. Finally, the energy of the detected radiation in an activation experiment is quite low since it mostly corresponds to decays between nuclear states which generally range between tens of keV to few MeV.

Concerning the ideal beam characteristics for an activation measurement, the energy should be known as accurately as possible. The beam intensity should be high enough to induce the highest activity in the sample in the shortest possible time to satisfy requirements for sufficient statistics and reasonable beam usage time. A steady beam intensity is also desirable, and at the very least, it must be possible to monitor beam fluctuations to make the appropriate corrections in the data analysis. Finally, a good alignment of the beam and sample is necessary in order to maximise the flux and reduce the uncertainty in the beam energy.

Finally, the sample characteristics are subject to various limitations. The sample size must be compatible with the beam-spot size which is generally of the order of a few to several millimetres in order to maximise the flux and minimise the energy uncertainty. At the same time, a larger number of target nuclei will increase counting statistics. The availability, cost, physical and chemical properties will also significantly affect the sample preparation and therefore its size and form. Radio-protection issues may arise if the induced and/or activity is too high. The target must not significantly alter the characteristics of the beam and if the macroscopic cross section of the sample for the detected particles is too high, leading to increased self-absorption, it is vital to minimise the thickness of the sample.

Chapter 2

Experimental

Irradiations of high-purity gold samples with quasi-monoenergetic neutron beams at energies between 9.0 and 10.5 MeV were carried out at the 5.5 MV Tandem Van de Graaff accelerator at the NCSR "Demokritos". Following the irradiations, the induced activity on the samples was measured with a 56% relative efficiency HPGe detector at the nuclear physics lab of the Department of Physics of the National Technical University of Athens.

2.1 The neutron beam

A quasi-monoenergetic neutron beam was produced via the ^{2}H(d,n)^{3}He reaction by bombarding a deuterium gas target with a deuteron beam at currents of around 1-2 μA. The gas target is fitted with a 5 μm molybdenum entrance foil and a 1 mm Pt beam stop and is constantly cooled with a cold air jet during irradiation to diminish the risk of damage to the Mo foil. The deuterium pressure was set to 1500 mbar. Using this setup, the achieved flux varied between 3×10^{5}-4×10^{6} n/(cm^{2}·s) in the four runs performed.

Particular attention was given to estimating the neutron energy distribution in the samples. The linearity of the selection magnet has been verified at low energies through the Al(p,γ) strong resonance at 991.91 keV and the ^{16}O(d,n) threshold reaction (E_{th}=1828.83 keV) leading to an estimate of the beam energy offset of 1.6 keV and a beam energy uncertainty of 0.1%. Assuming possible non-linearity at high energies, an overestimated beam energy uncertainty of 0.15% has been accepted to include possible second order effects.

A considerably more significant effect on the energy uncertainty of the produced neutrons is straggling from energy loss in the entrance foil and the deuterium target. Furthermore, as it was not possible to control the flow of deuterium in the gas cell remotely, the pressure was at times lower than the desired value by up to 200-300 mbar. These effects were estimated with the SRIM software [31] and the energy uncertainty value from straggling was less than 30keV. Finally, the angular acceptance of the target foils introduces additional uncertainty due to the ^{2}H(d,n)^{3}He reaction kinematics.

Taking the above into account, the appropriate adjustments were made, where possible, to ensure that the width of the neutron energy distribution in the samples did not exceed 50 keV.

The contribution of background "parasitic" neutrons was also studied in detail [2]. These neutrons originate from the interaction of the deuteron beam with the beam line structural materials, beam collimators and gas cell components. The multiple foil activation technique was implemented to determine the neutron beam profile. The appropriate foils were chosen in which neutron threshold reactions take place at different threshold energies and they were placed immediately after the Au and two Al foils for irradiation. Information from the Au and Al foils was also included in this analysis. The relevant reactions with their threshold energies are presented in Table 2.1.

The results of these irradiations were processed with the SULSA unfolding code [32]. A key feature of the code

Table 2.1: Reactions used for neutron beam profiling

	E_{th} (MeV)
^{58}Ni(n,p)^{58}Co	0.0
^{59}Co(n,α)^{56}Mn	0.0
^{47}Ti(n,p)^{47}Sc	0.0
^{115}In(n,$n^{'}$)^{115m}In^{m}	0.34
^{64}Zn(n,p)^{64}Cu	1.0
^{46}Ti(n,p)^{46}Sc^{g+m}	1.76
^{56}Fe(n,p)^{56}Mn	2.97
^{48}Ti(n,p)^{48}Sc	3.28
^{27}Al(n,α)^{24}Na	3.25
^{197}Au(n,2n)^{196}Au	8.11
^{93}Nb(n,2n)^{92}Nb^{m}	8.93

is that it does not require an input spectrum. By providing the activation rates measured for each foil, the code extrapolates the energy distribution of the beam using cross section values and covariance matrices from an incorporated library. Modifications were made to include additional reactions in the analysis.

The results of this analysis showed that, although a considerable population of background neutrons is produced during the irradiations, these lie mainly in the low-energy region, well below the threshold for the ^{197}Au(n,2n) (E_{th}= 8.11 MeV) reaction. As far as the ^{27}Al(n,α)^{24}Na reference reaction is concerned, while E_{th}= 3.25 MeV, the cross section only grows sufficiently to produce measurable activation rates at incident neutron energies above 6.8 MeV.

2.2 Irradiations

Four irradiations have been carried out, evenly spaced in the energy range between 9.0 to 10.5 MeV. Given that the cross section for the formation of the second isomeric state is significantly lower than that for the population of the ground state, the irradiations typically lasted approximately 24 hours, which corresponds to roughly 84% of the saturated activity of the second isomeric state. The saturated activity is the maximum attainable activity in the sample given the reaction rate which is defined by the cross section, the beam intensity and number of target nuclei and is therefore approximately constant. Once the decay rate becomes equal with the reaction rate, further irradiation of the sample is useless. While it takes theoretically infinite time to reach saturation, usually a good result is achieved after an irradiation of approximately 3 half-lives, if the corresponding beam time is practical.

High purity natural gold foils (99.99% ^{197}Au) with a diameter of 14 mm and thickness of 0.5 mm were used. Two Al foils of the same diameter and thickness were placed immediately before and after the gold foil and were used to determine the neutron flux. The Al foils were chosen to take advantage of the well known ^{27}Al(n,α)^{24}Na reaction cross section. The residual ^{24}Na nucleus decays by β_- decay to ^{24}Mg with a half-life of 15 h emitting a 1369 keV γ-ray.

The samples were placed at 0° with respect to the neutron beam and at a distance of 8 cm from the centre of the gas cell, thus limiting the angular acceptance of the target foils to ±5° minimising the energy uncertainty.

Beam fluctuations were monitored with a BF_3 counter placed at a distance of 3 m from the deuterium gas target. Following Monte Carlo simulations of the experimental area, the BF_3 unit was placed at an angle of 30° with respect to the beam line to avoid an increased presence of "parasitic" background neutrons near the target foils due to backscattering on the BF_3 setup. Data from the BF_3 counter were stored at regular time intervals (60 s) by means of a multi-channel scaler and were used to correct for the decay of ^{196}Au nuclei during irradiation and to account for fluctuations in the beam flux in the subsequent off-line analysis.

Table 2.2: Summary of the irradiation and off-line measurement parameters

	9.0 MeV	9.5 MeV	10.0 MeV	10.5 MeV
Irradiation time (h)	23.22	14.03	25.12	25.08
Integrated flux ($\times 10^{11}$) (cm^{-2})	3.45±0.19	0.27±0.02	4.62±0.18	0.33±0.02
Measurement time[1] (h)	10.96[2]/10.96	3.89/1.00	21.97/5.98	51.15/19.95
Decay correction f[1]	0.948/0.490	0.964/0.599	0.944/0.462	0.943/0.458
Decay correction D[1]	0.050/0.515	0.012/0.061	0.057/0.325	0.125/0.706

[1] Two values are given for these parameters: A/B. The A corresponds to the σ_{g+m1} and the B value to the σ_{m2} measurement.
[2] In this case, the contribution of the decay of the second isomeric state to the activity of the ground state was negligible due to the very low cross section, and the measurements were carried out simultaneously.

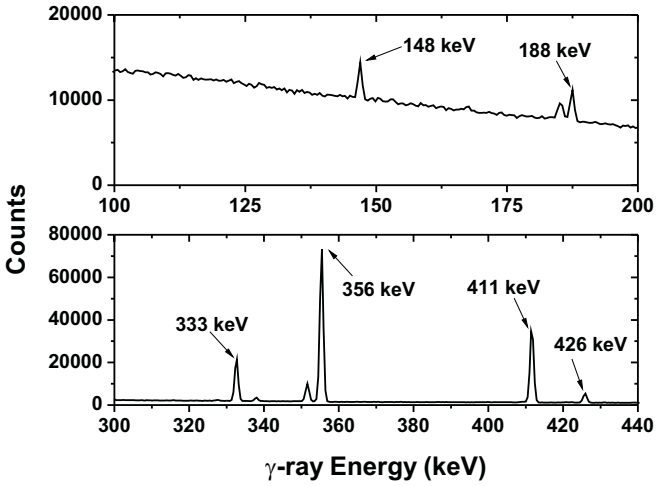

Figure 2.1: Experimental spectra from the decay of the second isomeric state (top panel) and ground state (bottom panel) of ^{196}Au, after irradiation at 10.5 MeV incident neutron energy. The acquisition time is 20 h and 51 h respectively.

The main quantities concerning the irradiations of the samples are summarised in Table 2.2.

2.3 Activity Measurements

Following the irradiations, the induced activity on the samples was measured with a 56% relative efficiency HPGe detector. The detector was calibrated with ^{152}Eu and ^{207}Bi sources, the latter being used to obtain a more accurate efficiency curve in the low-energy region. The samples were placed at a distance of 10 cm from the detector window. With this counting setup, corrections for coincidence summing become negligible. Figure 2.1 shows typical spectra acquired from the gold samples during the measurement for the second isomeric state (top panel) and the ground state (bottom panel), where the γ-rays of interest have been marked. The γ-ray intensities and half lives used in the analysis are summarised in Table 2.3.

The population of the second isomeric state was measured through the 148 keV line. This was preferred over the 188 keV line due to its higher intensity (45% over 30%) and the existence of a nearby natural background line (Fig. 2.1). These measurements began approximately 1 h after the end of the irradiation and lasted up to 20 h (two half-lives), depending on the evolution of the peak-to-background ratio. Following this, the activity of the Al foils was measured with the same experimental setup through the 1369 keV transition. For these measurements, a duration between 1 and 3 h was sufficient to achieve a statistical error lower than 2%.

Since the first isomeric state decays relatively very quickly ($T_{1/2}$ = 8.1 s), the measurements on the decay of the ground state result in the determination of the sum of the cross sections for the population of the ground

Table 2.3: Decay properties of the daughter nuclei

Daughter nucleus	Half-life	γ-ray energy	Intensity per decay (%)
^{196}Au^{g1}	6.1669±0.0006 d	333.0	22.9±0.9
		355.7	87±1
		426.1	6.6±0.1
^{196}Au^{m21}	9.7±0.1 h	147.8	43.5±0.1
		188.3	30.0±1.5
^{24}Na[2]	14.9590±0.0012 h	1368.6	100.0±0.0

[1] [3]
[2] [4]

state and the first isomeric state. Moreover, these measurements were carried out at least two days after the irradiation to ensure that the second isomeric state ($T_{1/2}$ = 9.7 h) had fully decayed to the ground state, since the correction for the contribution of the second isomeric state to the measured activity of the ground state was found to be negligible when the latter measurement was carried out after several half-lives of the second isomeric state.

The activity of the ground state was deduced through the 356 keV line, preferred over the 333- and 426 keV lines due to the much higher counting statistics (Fig. 2.1). Furthermore, the 333 keV line is contaminated by the 334 keV line of ^{198}Au arising from the ^{197}Au(n,γ)^{198}Au reaction. This is confirmed by the 411 keV line which is clearly visible in the acquired spectrum and also belongs to the (n,γ) channel.

2.4 Data Analysis

2.4.1 Cross section calculations

In each case, the experimental values of the cross sections were determined through the following formula:

$$\sigma = \frac{N_\gamma}{\epsilon I N_T \Phi S f D} \tag{2.1}$$

where N_γ is the number of counts in the relevant γ-ray peak. The factor ϵ is the detector efficiency, I is the γ-ray intensity, N_T is the number of target nuclei and S is the self-absorption correction factor. Decays during irradiation and time fluctuations in the beam flux are accounted for with the correction factor f, given by:

$$f = \frac{\int_0^{t_b} e^{-\lambda t} F(t)\, dt}{\int_0^{t_b} F(t)\, dt} e^{-\lambda t_b}, \tag{2.2}$$

where t_b is the irradiation time and $F(t)$ is the beam flux in arbitrary units as given by the BF_3 counter, while D corrects for the interval between the end of the irradiation and the end of the measurement and is given by:

$$D = (1 - e^{-\lambda t_m}) e^{-\lambda t_w}, \tag{2.3}$$

where t_w and t_m are the waiting time between irradiation and measurement and the measurement time respectively. The integrated neutron flux Φ was determined through the same formula (Eq. 2.1) by using the cross section values for the ^{27}Al(n,α)^{24}Na reaction found in literature [5] and by averaging over the deduced values in the front and back Al foils. It is thus possible to correct for target geometry and self-shielding.

Table 2.4: Experimental uncertainties

	Uncertainty (%)
Neutron energy	<1
Neutron flux[1]	4-6.5
Correction factors	2
Time factors	<0.5
Counting statistics[2]	0.2-1.2/4.2-15.1[3]
γ-ray intensity per decay[2]	1.1/0.2
Detector efficiency	5
Total uncertainty of cross section	7.3-8.7/8.3-17.7[3]

[1] Including 2% uncertainty in the ^{27}Al(n,α)^{24}Na cross section
[2] Two values are given for these parameters: A/B. The A corresponds to the σ_{g+m1} and the B value to the σ_{m2} measurement.
[3] The value of the counting statistics uncertainty is 41.5% for the 9.5 MeV run, due to the low beam current and shorter than desired irradiation, leading to a total cross section uncertainty of 42.4%.

The experimental uncertainties of all the factors used in equation 2.1 were summed quadratically in order to obtain the total cross section errors and are summarised in Table 2.4.

2.4.2 Self-absorption corrections

Given the relatively low energy of the γ-rays of interest and the high mass attenuation coefficient of gold, it was essential to take self-absorption effects into consideration. A Monte Carlo simulation of the counting geometry using the MCNP code [6] was performed to estimate this correction. The simulated geometry can be seen in fig. 2.2. Photons of the desired energy are generated homogeneously inside the sample and the number of photons crossing a circular area corresponding to the front face of the Ge crystal is recorded. The simulation is performed twice, the second time having removed the material from the target, in order to isolate the contribution of self-absorption from the solid angle, which is already accounted for in the determination of the detector efficiency. Finally, the self-absorption coefficient is calculated as:

$$S = \frac{S_{mat}}{S_{void}} \tag{2.4}$$

Approximately 55% of the 148 keV and 12% of the 356 keV line are lost due to self-absorption in a 0.5 mm -thick gold foil. Self-absorption of the 1369 keV line in Al was found to be less than 0.5%.

2.5 Results

The new experimental data produced can be seen in figures 2.3, 2.4 along with previous data found in literature. These results are discussed in chapter 5.

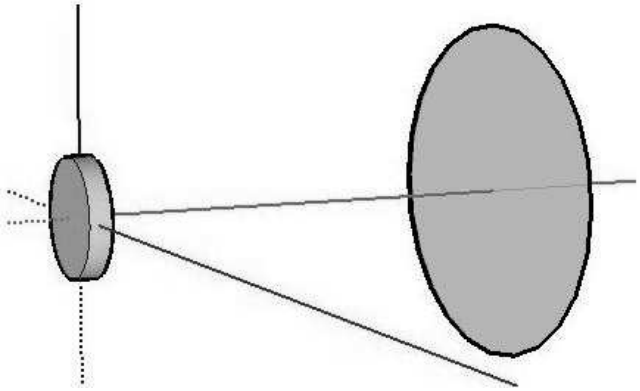

Figure 2.2: The Au sample and the front face of the HPGe detector as implemented in the MCNP simulation for the estimation of the self-absorption correction (dimensions not to scale).

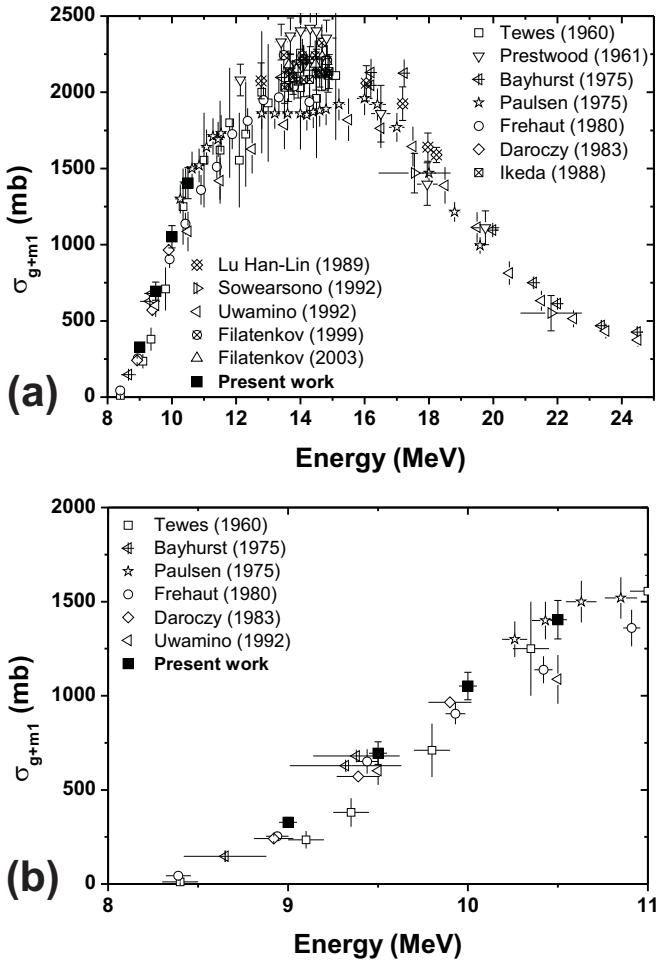

Figure 2.3: Experimental results of present work and previous experimental data for the population of the ground and first isomeric state of ^{196}Au (g+m1) between 8-25 MeV (a) and 8.5-11 MeV (b). Several datasets around 14 MeV have been omitted for clarity.

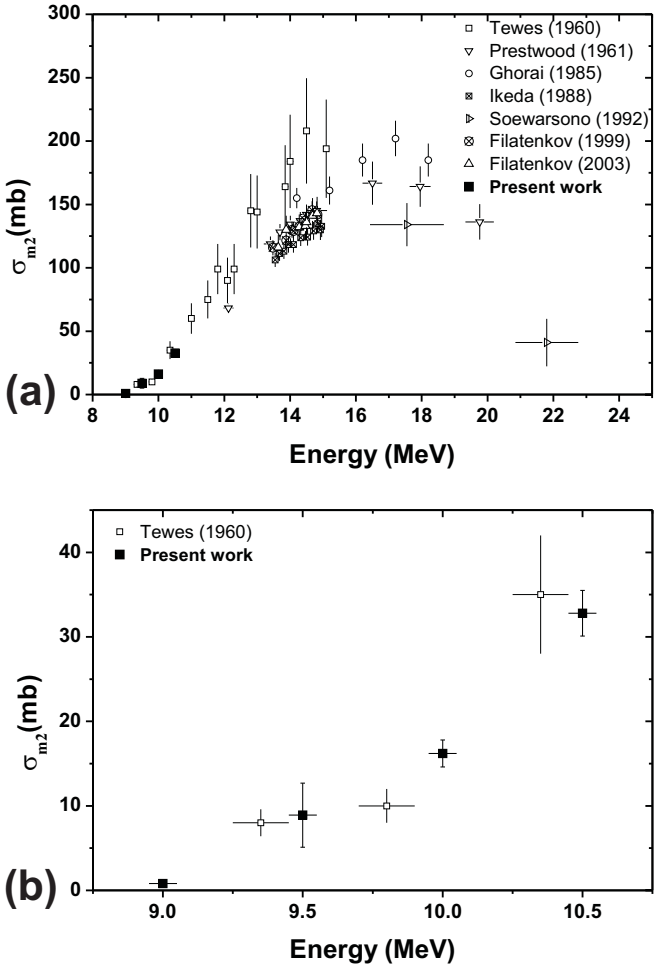

Figure 2.4: Experimental results of present work and previous experimental data for the population of the second isomeric state of ^{196}Au (m2) between 8-25 MeV (a) and 8.5-11 MeV (b).

Part II

Theoretical Calculations

Chapter 3

Nuclear reaction and nuclear level density models

3.1 Nuclear reaction mechanisms

Depending on the manner in which the projectile and target interact, nuclear reactions can be broadly sorted into three categories: *direct*, *pre-equilibrium* and *compound nucleus* reactions. In a direct reaction, the projectile interacts with only a few of the target nucleons and the reaction products are emitted very quickly. In compound nucleus reactions, the projectile and target form a compound nucleus that reaches thermodynamic equilibrium before decaying into the reaction products. Pre-equilibrium reactions are an intermediate case, where reaction products are emitted before thermodynamic equilibrium of the projectile-target system has been fully reached.

It should be noted that all reactions mechanisms contribute to a specific reaction, to a different extent. This is dependent on several factors, such as the projectile energy and charge, the mass of the projectile and target and the structure of the projectile-target system (energy levels, excitation, spin distributions etc.). Theoretical models for the description of each of these mechanisms have been developed over the years.

3.1.1 Direct reactions and pre-equilibrium emission

For a direct reaction to take place, the projectile must have a wave-length $\lambda \approx$1fm in order to interact with single nucleons. Obviously, therefore, the probability of a direct reaction increases with the projectile energy. Furthermore, the angular distribution of reaction products is strongly forward-peaked relative to the incident particle direction. Typically, direct reactions last approximately 10^{-22}s, which roughly corresponds to the time necessary for the projectile to traverse the target nucleus. Knock-out reactions, (in)elastic scattering, (d,p) and (p,d) reactions are typical examples of direct reactions.

The so-called *optical model* is commonly used to describe direct reactions. The optical model describes the nuclear reaction as the interaction of the incoming particle with a complex potential $V(r) = -V - iW$, where the real part corresponds to scattering and the imaginary part to absorption. The model bears a direct analogy to light being scattered and/or absorbed by a dark sphere.

Should the incident particle have the time to interact with a few of the target nucleons, then a composite system begins to form and the energy of the projectile is (partially) shared with neighbouring nucleons through nucleon-nucleon interactions. It is possible, however, that, as the system passes through a series of states of increasing complexity, one or more of these nucleons might acquire enough energy to be emitted from the nucleus before full equilibrium has been reached. This is called a pre-equilibrium reaction.

3.1.2 The compound nucleus reaction mechanism

The compound nucleus reaction mechanism is based on the assumption that the reaction takes place in two distinct steps. First, the projectile enters and is captured by the target nucleus forming a compound system. Through a large number of nucleon-nucleon interactions, the energy of the incident particle is shared among all nucleons until equilibrium is reached. Statistical fluctuations may lead one or more nucleons or light nuclei to acquire energy higher than the average energy increase and sufficient to overcome the nuclear potential if they are found near the surface of the nucleus, much like the evaporation of molecules from the surface of a drop of liquid. It is obvious that neutrons will be emitted with greater ease, being insensitive to the Coulomb potential of the nucleus. In the second step, the compound nucleus decays into the reaction products, either by emitting further particles, if there is sufficient available energy, or through γ-decay.

The manner of de-excitation of a compound system is independent of the way in which it was formed (the entrance channel), but only depends on the energy, spin and parity it has acquired. In other words, the process of reaching equilibrium through a large number of energy transfers between nucleons is considered to "erase the memory" of the system. This is often referred to as the Bohr hypothesis. Some obvious consequences of this are that the angular distribution of the reaction products is isotropic, since "memory" of the original direction of the projectile has been lost. Furthermore, the same compound nucleus can be formed via different entrance channels, but still decay through the same exit channel.

The limits of validity of the Bohr hypothesis can be outlined as follows. In order to reach equilibrium, the projectile will need to transfer its energy to the target nucleons it encounters relatively quickly, before it can escape the nucleus. This depends on the projectile energy and the size of the target nucleus. This requirement can be expressed with two conditions. First, the mean free path L of the projectile in the target (i.e. the distance it will travel before it loses its excess energy and acquires the average nucleon energy) should be much smaller than the size of the target nucleus or its radius R. Second, a large number of interactions should be necessary before the emission of a nucleon.

Assuming that the excitation energy $E_{ex} = E_{kin,a} + S_a$ is equally distributed among nucleons, who will each receive energy E_{ex}/A, we can require this energy to be lower than the separation energy S of a nucleon. In the common case where the projectile is a nucleon or light nucleus, when $S \approx S_a$, we can then require that $L \ll R$ and $E_{ex}/A \ll S \Leftrightarrow E_{kin,a} \ll (A-1)S$.

From the above, and given that typically $S \approx 8$ MeV it becomes clear that the compound nucleus mechanism becomes important when the target nucleus is relatively heavy ($A > 10$) and the projectile energy is in the MeV region.

The theoretical cross section calculations on the ^{197}Au(n,2n) reaction were performed in the energy region between 8 and 25 MeV, taking into account the compound mechanism and pre-compound contributions in the framework of the Hauser-Feshbach theory [7] and the exciton model [8] respectively.

3.2 Nuclear level density

In the previous sections, the energy states of the compound nucleus were tacitly assumed to form a continuum where the average energy difference D between two neighbouring states is much smaller than the width Γ of these states. This is true at high excitation energies. Since individual states cannot be distinguished, the nuclear continuum is described not by discrete states, but by a level density $\rho(U, J, \pi)$. On the contrary, discrete levels found at lower excitation energies can be studied experimentally and their energy, spin and parity determined.

Several level density models have been proposed, each attempting to describe the continuum through a number of parameters whose values are generally determined through comparison with experimental data. Such are the Fermi Gas Model (FGM), the Constant Temperature Model (CTM), the Gilbert-Cameron model (GCM) and the Generalised Superfluid Model (GSM). In all cases it is assumed that the dependence of the level density from energy, spin and parity can be studied separately so that $\rho(U, J, \pi) = \rho(U)f(J)\rho(\pi)$, where $\rho(\pi) = 1/2$, since both parity values (± 1) are considered to be equally distributed in the continuum.

The level densities of the nuclei involved in the calculations for the ^{197}Au(n,2n) reaction were treated within the GSM in its phenomenological version developed by Ignatyuk et al. [9, 10]. Expanding upon the relatively simpler formalism of previous models, the GSM takes into account additional effects such as superconductive pairing correlations, shell effects and collective enhancement of the level density of the nucleus. It has already been successfully used in the past for theoretical cross section calculations in ^{191}Ir [11], which also lies in the transitional Os-Pb region.

3.2.1 The Generalised Superfluid Model (GSM)

Within the GSM, the key quantities used to describe the excited nucleus are not considered as constant, but rather as functions of nuclear temperature. Furthermore, the function itself changes between the low- and high-energy range (the superfluid and normal phase respectively) which are defined by a critical excitation energy U_{cr}. The critical nuclear temperature value t_{cr} is given by $t_{cr} = 0.567\Delta_0$, where $\Delta_0 = 12/\sqrt{A}$ is the pairing correlation function.

The level density $\rho(U, J)$ is treated separately in these two energy regions depending on the nuclear temperature t. The dependence of the level density on the excitation energy and spin can be separated as $\varrho(U, J) \propto \rho(U)f(J)$, where $f(J) = R(2J + 1)e^{-J(J+1)/2\sigma^2_{eff}}$ is the spin distribution function.

For $t < t_{cr}$ (or $U' < U_{cr}$) the nucleus is in the superfluid phase, where $\rho(U')$ is the level density of quasiparticle excitations in the Bardeen-Cooper-Schrieffer (BCS) theory [33], expressed in terms of the effective excitation energy $U' = U + n\Delta_0$, where U is the true excitation energy of the compound nucleus and n = 0, 1, 2 for even-even, even-odd and odd-odd nuclei. The level density parameter is considered constant in the superfluid phase of the nucleus ($\alpha = \alpha_{cr}$).

For $t \geq t_{cr}$ (or $U' \geq U_{cr}$) the nucleus is in the normal phase, where the pairing correlations vanish and the level density follows the simple parametrisation of the Fermi Gas Model [34] with a shift in the excitation energy by $E_{cond} = (3/2\pi^2)\alpha_{cr}\Delta_0^2$, which is the condensation energy characterising the decrease of the ground state of the Fermi gas because of the correlation interaction. The level density parameter α varies with energy according to the equation:

$$\alpha = \tilde{\alpha}[1 + \frac{\delta\epsilon_0}{U' - E_{cond}} f(U' - E_{cond})] \tag{3.1}$$

where $\tilde{\alpha}$ is the asymptotic value of α at high excitation energy and $\delta\epsilon_0$ is the shell correction of the nuclear binding energy. The dimensionless function $f(U')$ determines the energy behaviour of α for the normal phase [10].

3.3 Nuclear reaction codes

The theoretical calculations were carried out using three nuclear reaction codes, STAPRE-F [12], EMPIRE 2.19 [13] and TALYS-1.2 [14]. Some important details on each are given below.

The choices for the transmission coefficients, the pre-equilibrium and the level densities used for the calculations of the three codes were made in order to compare how the three codes implement the generalised superfluid model. The STAPRE-F code provides a local approach in which a consistent calculation is made using local model parameters established on the basis of various independent data, while EMPIRE and TALYS provide global approaches of the nuclear models included [15, 35].

3.3.1 STAPRE-F

The STAPRE-F code is designed to estimate energy averaged cross sections for particle-induced reactions with several possible emitted particles (n, p, α, d) and γ-rays, under the assumption of sequential evaporation. For each evaporation step the statistical model is used with respect to energy, angular momentum and parity

Table 3.1: Statistical model calculation parameters for STAPRE-F

Parameter	^{198}Au	^{197}Au	^{196}Au	^{195}Au	Ref.
$\tilde{\alpha}$ (MeV^{-1})	16.827	16.736	16.645	16.554	[38]
$n\Delta_0$	1.706	0.855	1.714	0.859	[12]
$\delta\epsilon_0$	-4.392	-3.580	-2.931	-2.292	[38], [39]
ϵ,quadrupole deformation parameter	-0.131	-0.131	-0.139	-0.139	[40]
Neutron separation energy (MeV)	6.45	8.07	6.64	8.38	[41]
Average experimental total radiation width (meV)	128	120[1]	93[1]	70[1]	[38]

[1] These values were not included to the average parameters of s- and p- wave neutron resonances provided by A. V. Ignatyuk, and were deduced according to the values for neighbouring nuclei.

conservation. In the present work, only the contribution of neutrons and γ-rays was taken into account for the Hauser-Feshbach denominator because the charged particle emission is inhibited by the Coulomb barrier.

The neutron transmission coefficients were calculated using the ECIS03 code [36] with the global optical model parameters by Koning and Delaroche [37], as the gold isotopes in question are slightly deformed (as indicated by the quadrupole deformation parameter ε in Table 3.1).

For the first evaporation step pre-equilibrium decay is taken into consideration within the context of the exciton model. The pre-equilibrium emission factor is determined by the square matrix element $|M|^2 = KA^{-3}E^{-1}$, where A is the mass number of the target nucleus, E is the energy of the incident particle and K is the free parameter of the model, which can be estimated by the hard component of the inelastically scattered neutrons or from the shape of the excitation function of (n,2n) or (n,3n) reactions. In the present work, the value of 200 was used for K.

The γ-ray strength functions for M1, E2, M2 and E3 were calculated according to the Weisskopf model, based on the single particle estimation and normalised to the E1 strength function which was calculated according to the Brink-Axel hypothesis [42, 43]. The E1 strength function was normalised to reproduce the experimentally observed average radiation width $< \Gamma_\gamma >$ at the neutron binding energy [38].

The GSM parameters used in the calculations were taken from literature and are summarised in Table 3.1. For the perpendicular moment of inertia of the ground state of the nuclei involved the empirical estimate $\Theta_{rig}/3$ was used in consistency with the ground state rotational bands of ^{196}Pt and ^{196}Hg.

The energies, spins, parities and branching ratios of the discrete levels for each nucleus involved were taken from Nuclear Data Sheets [3], and the first 90 levels of ^{196}Au were included (up to ~ 0.730 MeV). For the levels with unknown spin and parity, estimates from neighbouring levels were made, while for levels with more than one spin assignment, a choice was made in order to include a variety of spin values.

3.3.2 EMPIRE

EMPIRE-II is a modular system of nuclear reaction codes, implementing the major reaction mechanisms, such as compound nucleus (in the Hauser-Feshbach model with width fluctuation correction [44]), pre-equilibrium emission (by means of the exciton model or the Hybrid Monte-Carlo Simulation approach) and direct interaction (using various optical model parameters automatically retrieved from the RIPL-2 library [38] or chosen by the user). In the present work, version 2.19 was used with the default parameters concerning nuclear masses, ground state deformations, discrete levels, decay schemes and strength functions.

The emission of neutrons, protons, and α-particles is automatically taken into account in competition with full γ-cascade in the residual nuclei. The particle transmission coefficients were calculated using the ECIS03 code [36], using the optical model parameters by Koning and Delaroche [37] for neutrons and protons and the default parameters of [45] for α-particles. The pre-equilibrium contribution was taken into account via the exciton model as implemented in the EMPIRE-II code (DEGAS) [13].

For the description of the level density in the continuum, the so-called dynamic approach of EMPIRE-II was used. This includes the superfluid model formalism [9] adjusted to experimental values of the level density parameter α and to discrete levels for $U' < U_{cr}$, and the Fermi gas model above U_{cr}.

3.3.3 TALYS

The TALYS-1.2 code is also a modular system of a variety of nuclear models for direct, compound, pre-equilibrium and fission reactions, phenomenological and microscopic level density models and automatic reference to libraries (RIPL-2 [38]) for the nuclear structure parameters needed in the calculations. All the reaction chains are followed until all possible exit channels are closed, leading to their ground or an isomeric state.

The default values were used for parameters concerning nuclear masses, ground state deformations, discrete levels (except for the number of discrete levels included in the Hauser-Feshbach calculations which was increased to accommodate the second isomeric state of ^{196}Au), decay schemes and strength functions [42, 43, 46].

The particle transmission coefficients were calculated via the ECIS-06 code [36] using the default optical model parameters by Koning and Delaroche [37]. The pre-equilibrium contribution in the first step of the nuclear reaction was calculated via the default exciton model incorporated in TALYS [47]. The GSM level densities were selected with all the default parameters of the code. The explicit collective enhancement of the level density was enabled, and the level density parameters were taken from the systematics for reasons of consistency with the other codes.

Chapter 4

Initial results and investigation

4.1 Initial results

The theoretical calculations obtained from the three codes for σ_{g+m1} and σ_{m2}, along with the data from this work and the previous measurements are presented in figures 5.1 and 5.2.

As seen in Fig. 5.1, the results from all three codes fairly reproduce the trend of the experimental data for σ_{g+m1}. The theoretical curves appear to span the whole range of the experimental values in the 12-16 MeV region where large discrepancies in the data exist. This precludes a conclusion on the accuracy of the results in this region.

Concerning the cross section of the second isomeric state (Fig. 5.2) the STAPRE-F and EMPIRE theoretical calculations seem to underestimate the near-threshold data up to about 13 MeV, while in the high-energy region they overestimate the cross sections by about 100 mb, despite the large discrepancies among the experimental data. The TALYS calculation underestimates the data in the whole energy range, a behaviour also encountered in [15]. Furthermore, in all cases the cross section attains its maximum value at around 18 MeV, about 2 MeV higher than the experimental data suggests. This result will be discussed later. Nevertheless, all three codes reproduce the general trend of the experimental data.

4.2 Further tests

Based on the observations described earlier, several tests were made, using the available codes.

STAPRE-F provides the user with wide liberty in changing the various parameters, as opposed to EMPIRE and TALYS where most values are retrieved from existing libraries. For this reason, the sensitivity of the results to several theoretical parameter values was studied using the STAPRE code.

The implementation of level density models alternative to the GSM is not possible in STAPRE-F, but it is very straightforward in EMPIRE. Tests concerning the addition of discrete levels were handled with STAPRE-F, while results from manipulation of the nuclear moment of inertia can be obtained with both codes. Details of the tests performed with STAPRE-F can be found in [16].

4.2.1 Theoretical input parameters

The tests made with STAPRE-F in order to better reproduce the isomeric cross section results consisted in changing the input parameters of the theoretical calculations and accounting for the (n,3n) reaction which becomes important above 16 MeV [48–50]. Particular attention was given to the value of $\tilde{\alpha}$ (Table 3.1) which is the level density parameter at high excitation energies (Eq. 3.1) and plays an important role in the calculations.

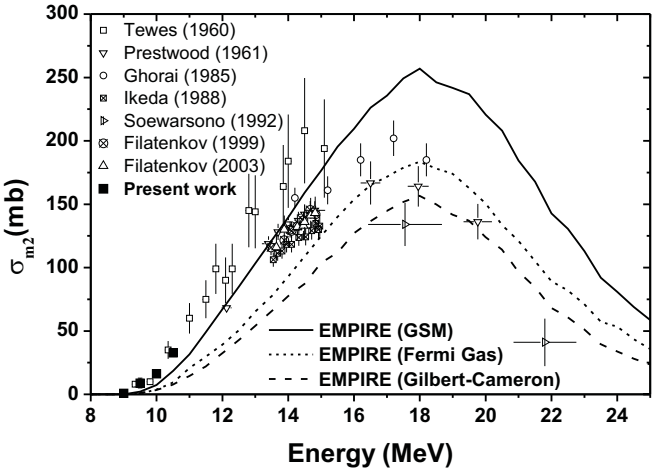

Figure 4.1: Theoretical calculations for σ_{m2} using the Fermi gas and Gilbert-Cameron level density models, compared to the result using the GSM.

Initially, these values were changed in a consistent way within their experimental uncertainties (i.e. $\pm$ 6 %) for $^{195-198}$Au isotopes. Subsequently, the $\tilde{\alpha}$ values for these isotopes were changed in order to follow the systematics proposed in [38, p.103], where α at the neutron separation energy is up to 20% lower than those given by Eq. 3.1 and decreases with increasing A.

Nevertheless, none of these attempts seemed to simultaneously improve the fit to the experimental data of σ_{m2}, σ_{g+m1} and the cross section values of the (n,3n) reaction. Furthermore, the average experimental total radiation width and the moment of inertia of the ground state were changed within their experimental uncertainties, as was the percentage of pre-equilibrium emission and the assumptions on the shape and symmetry of the Au isotopes, but the effect on σ_{m2} was within 10%, and the theoretical curve remained shifted to higher energies.

4.2.2 Model dependence

In order to understand and correct the shift of the σ_{m2} theoretical curve, which is shifted to higher energies compared to the experimental data as mentioned before, this discrepancy was investigated to check whether this behaviour is dependent on the level density model being used (the GSM).

Since EMPIRE offers the possibility of easily switching between level density models, the calculations were repeated using the Back Shifted Fermi Gas [17] and the Gilbert-Cameron level density models [18] using EMPIRE, and leaving the rest of the input parameters as mentioned above. The results (Fig. 4.1) show that the shift of the isomeric cross section curve is independent on the model of the level density of the nuclei involved. In addition, it can be seen in Fig. 5.2 that it is also independent on the implementation of the GSM in the three codes used.

4.2.3 Moment of inertia

Generally, the population of the high spin isomers is highly dependent on the spin distribution of the continuum. The effect of this factor on the feeding of the 12^- isomer was examined in order to improve the theoretical predictions.

In previous cross section measurements of high spin isomers in nuclei belonging to the transitional region from the well deformed Os to the spherical Pb isotopes [11, 19–21] the need of the reduction of the effective moment of inertia was pointed out, in order to better reproduce the data of σ_{m2} and the isomeric ratio. Furthermore, in the framework of the Back-Shifted Fermi Gas Model (BSFGM), systematics have been evaluated for the mass dependence of the reduction of the effective moment of inertia with respect to the rigid body value [51] which have been proved quite satisfactory in an extended mass region, even in the heavy Hg and Au isotopes [19].

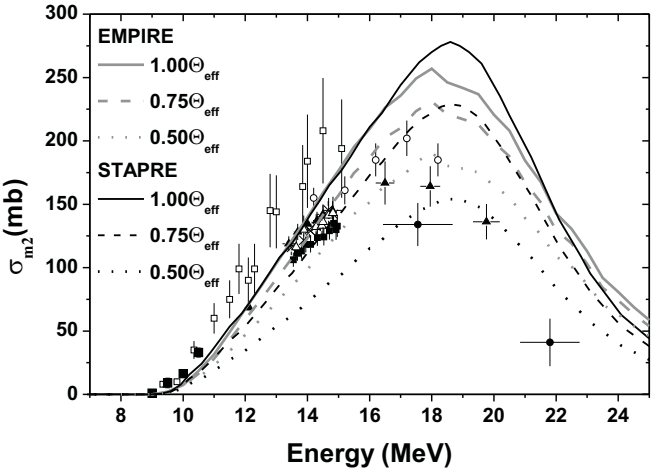

Figure 4.2: Theoretical calculations for σ_{m2} using values of the effective moment of inertia reduced by 25 and 50%.

The same result has occurred in the framework of the GSM for the Ir isotopes as reported in [11], where the effective moment of inertia had to be reduced to 75% of the rigid body value in order to better reproduce the trend of the data. The BSFGM and GSM have the same spin distribution shape and from the previous discussion one would also expect a similar systematic behaviour of the spin cutoff parameter within the GSM, i.e. the need for a similar reduction of the effective moment of inertia for the reproduction of the data for Au. In order to test this idea, theoretical calculations were carried out using Θ_{eff} values lowered by 25 and 50% using the STAPRE-F and EMPIRE codes, and the results are presented in Fig. 4.2. The reduction of the effective moment of inertia causes a significant decrease of the isomeric cross section but does not seem to improve the theoretical results with reference to the experimental data, as in the neutron energy region below 14 MeV the theoretical calculations are already lower than the experimental data, and as a result the lowering of Θ_{eff} causes a further deviation from the data. In the high energy region the theoretical predictions move closer to the experimental data but retain the maximum cross section value around 18 MeV in contrast with the data.

This result indicates that the reduced value of Θ_{eff} cannot improve the theoretical results and, given also the existing shift of the curve to higher energies, the hypothesis of possible discrepancies in the level scheme was examined. In particular, the level schemes of ^{196}Au and ^{195}Au are expected to play a crucial role in the cross section value of the 12^- isomer and are discussed below.

4.2.4 Level schemes

The level scheme of ^{196}Au, especially the spins of levels lying above the 12^- isomer are very important for the feeding of this level [22, 52] in the whole neutron energy range. The existence of the 12^- isomer among the low-lying excited states results from the high spin intruder configurations πh11/2$\otimes\nu$i13/2 [27] and inhibits its communication with neighbouring states. The possible existence of a rotational band built on this intrinsic structure for doubly odd nuclei in this region is proposed in [53] and [54], and rotational bands based on high-j unique parity quasi-particle states (πh9/2, πh11/2, νi13/2) have been reported for Tl isotopes in [53] and other isotopes in the transitional region Os-Pb (references in [54]), as well as dipole bands in Pb and Hg isotopes [55–58]. The possible existence of a rotational band built on the 12^- isomer and feeding it through gamma cascade would increase the calculated cross section, and lead to a better reproduction of σ_{m2} at incident neutron energies below 16 MeV. In a similar case, the existence of a rotational band built on the configuration of the 16^+ isomer of ^{178} Hf has been proposed in [22] in order to successfully reproduce, within the Hauser Feshbach theory, the cross section values of the ^{179} Hf(n,2n) reaction that leads to its formation and was experimentally observed some years later via the incomplete fusion ^{176}Yb(^{9}Be,α 3n) ^{178}Hf reaction [23].

The level scheme of ^{195}Au is also expected to play an important role in the neutron energy region above 16

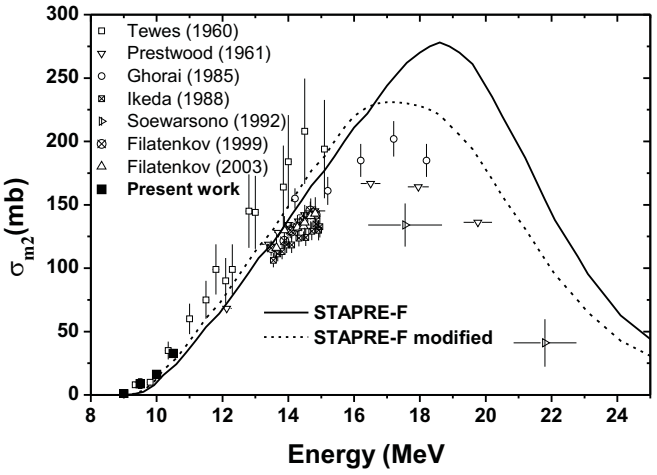

Figure 4.3: Theoretical calculations for σ_{m2} using a modified level scheme for ^{196}Au and ^{195}Au including hypothetical high-spin levels.

MeV, where the (n,3n) channel becomes important and where the largest deviation from the experimental data occurs. An examination of the level scheme of ^{195}Au in comparison with the level schemes of neighbouring odd Au isotopes ([24–26]) indicates a possible absence of high spin rotational band members from the documented levels. More precisely, in the level schemes of both ^{189}Au and ^{191}Au, $\Delta J = 2$ rotational band members have been observed, with spins from $\frac{11}{2}^-$ to $\frac{55}{2}^-$, energies up to approximately 6 MeV and a band-crossing around $\frac{31}{2}^-$, following a systematic trend. The same trend is followed by reported levels of ^{193}Au up to the energy of 4 MeV, while for ^{195}Au only the first three states are reported (with spins up to $\frac{19}{2}^-$ and energies up to 1.5 MeV). The introduction of such high spin states in the level scheme of ^{195}Au would lead to an increase of the de-excitation of the continuum of ^{196}Au towards these states, and thus a reduction of the theoretical σ_{m2} values above an incident neutron energy of 16 MeV.

Although the above assumptions on the level schemes of ^{196}Au and ^{195}Au seem physically likely, there is no possibility of embedding discrete levels in the continuum of the nuclei of interest via any of the three codes in order to further investigate this hypothesis and extract safe results.

The only test that could be performed was the addition of a few high spin levels in the discrete via the STAPRE-F code implementation and the results seemed encouraging. More specifically as far as the level scheme of ^{196}Au is concerned, several levels with spins $12^{\pm}$,$13^{\pm}$,$14^{\pm}$ have been added above the 12^- isomer and up to about 0.730 MeV where the continuum starts, feeding the isomer through gamma cascade. The result was a 10 % enhancement of σ_{m2} without altering the g+m1 and (n,3n) cross section values. In addition, in order to improve the σ_{m2} values in the high energy region, a further addition of levels with high spins between $\frac{17}{2}^-$ and $\frac{27}{2}^-$ in the discrete of ^{195}Au was tried, which simultaneously reduced the σ_{m2} by 10 % in the energy region above 16 MeV, as expected, and moved the maximum of the curve towards lower energies. The results of these two tests are shown in Fig. 4.3. Higher spins than those used in the tests, attributed to rotational bands, are expected to lie in the higher energy part of the continuum, which has a high spin distribution and part of it de-excites by feeding them. However, within the implementation of a code, the introduction of such high spin levels in the discrete is not expected to significantly affect the results, since their feeding from the high spin distribution part of the continuum would be negligible due to the large energy difference.

Chapter 5

Final results and conclusions

5.1 Experimental results

The cross section of the (n,2n) reaction on ^{197}Au, was measured independently for the population of the second isomeric state (σ_{m2}), and for the sum of the reaction cross section for the population of the ground and the first isomeric state (σ_{g+m1}). The cross section values were determined by means of the activation technique in the incident neutron energy range 9.0-10.5 MeV. The experimental results of this work are presented in Table 5.1 along with their uncertainties. As seen in figure 5.1, the data for the ^{197}Au(n,2n)^{196}Au^{g+m1} cross section are in good agreement with previous measurements.

The new data for the second isomeric state presented in this work (fig. 5.2) report significantly lower uncertainties (10-11% for the 10.0 and 10.5 MeV measurements compared to 20% in the other data within this range), barring the non-optimal 9.5 MeV measurement. Moreover, the measurement at 9.0 MeV is the only one carried out at this energy, so close to the threshold. The uncertainty in the incident neutron energy has also been reduced compared to the previous data, as described in subsection 2.1.

5.2 Theoretical calculations

Theoretical calculations in the energy range 8-25 MeV were performed with the use of three different codes (STAPRE-F, EMPIRE 2.19 and TALYS-1.2) taking into account all available experimental data. The exciton model and Hauser-Feshbach theory were employed for the pre-compound and compound processes respectively. The Generalised Superfluid Model was chosen for the description of the level density of the nuclei involved. The σ_{g+m1} cross section was easily reproduced by the calculations, while for σ_{m2}, the theoretical results could only reproduce the general trend of the experimental data, with the distribution being shifted to higher energies. Several tests were performed to improve the theoretical predictions.

Table 5.1: Experimental values for the ^{197}Au(n,2n)^{196}Au^{g+m1} and ^{197}Au(n,2n)^{196}Au^{m2} reaction cross sections and the isomeric cross section ratio

Energy (MeV)	σ_{g+m1} (mb)	σ_{m2} (mb)	$\sigma_{m2}/\sigma_{g+m1}$
9.0	328±26	0.8±0.1	0.0024±0.0003
9.5	695±60	8.9±3.8	0.013±0.006
10.0	1052±73	16.2±1.6	0.015±0.002
10.5	1404±102	32.8±2.7	0.023±0.003

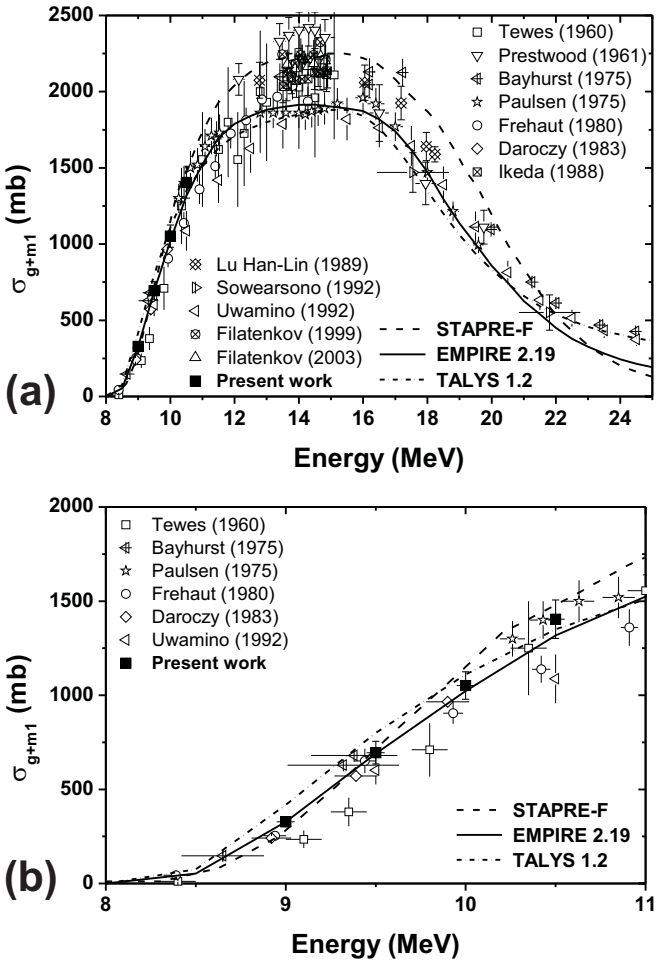

Figure 5.1: Experimental values and theoretical calculations for the population of the ground and first isomeric state of ^{196}Au (g+m1) between 8-25 MeV (a) and 8-11 MeV (b). Several single-point datasets around 14 MeV omitted for clarity.

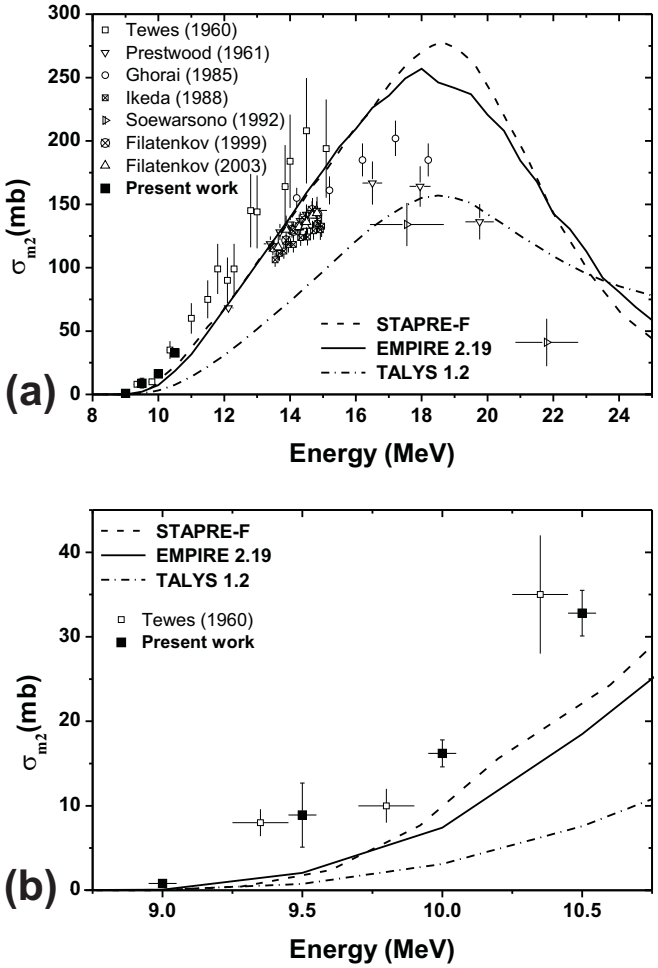

Figure 5.2: Experimental values and theoretical calculations for the population of the second isomeric state of ^{196}Au (m2) between 8-25 MeV (a) and 8.5-11 MeV (b).

5.3 Conclusions

The results of these tests reveal the importance of the level scheme of the residual nuclei and indicate the possibility of incomplete documentation of high-spin levels in the level schemes of ^{196}Au and ^{195}Au. Furthermore, they highlight certain limitations of the nuclear codes used, particularly regarding the embedding of discrete states in the continuum, which is not currently possible and affects the reproduction of high-spin isomeric cross sections.

The experimental search of the high-spin states in ^{196}Au and ^{195}Au that are apparently missing from available libraries as well as future experimental and theoretical work on other high-spin isomeric pairs in the same mass region would be of great interest. Finally, from a software point of view, the ability to treat discrete states inside the continuum would significantly benefit the precision and range of applicability of existing nuclear reaction codes.

Bibliography

[1] A. Tsinganis, M. Diakaki, M. Kokkoris, A. Lagoyannis, E. Mara, C. T. Papadopoulos, and R. Vlastou. Isomeric cross section of the ^{197}Au$(n, 2n)$ reaction. *Phys. Rev. C*, 83:024609, Feb 2011.

[2] R. Vlastou, M. Kokkoris, M. Diakaki, Ch. Constantinou, C.A. Kalfas, A. Kotrotsou, A. Lagoyannis, M. Lambrou, V. Loizou, E. Mara, V. Paneta, G. Provatas, and A. Tsinganis. Characterization of the neutron flux distribution at the Athens Tandem Accelerator NCSR "Demokritos". *Nuclear Instruments and Methods in Physics Research Section B: Beam Interactions with Materials and Atoms*, 269(24):3266 – 3270, 2011. Proceedings of the 10th European Conference on Accelerators in Applied Research and Technology (ECAART10).

[3] Huang Xiaolong. *Nuclear Data Sheets*, 108:1093, 2007.

[4] Richard B. Firestone. *Nuclear Data Sheets*, 108:2319, 2007.

[5] A.D. Carlson, R.C. Block, J.B. Briggs, E.T. Cheng, H.C. Huria, M.L. Zerkle, K.S. Kozier, A. Courcelle, V. Pronyaev, and S.C. van der Marck. *Nuclear Data Sheets*, 107:2391–3060, 2006.

[6] F. B. Brown, R. F. Barrett, T. E. Booth, J. S. Bull, L. J. Cox, R. A. Forster, T. J. Goorley, R. D. Mosteller, S. E. Post, R. E. Prael, E. C. Selcow, A. Sood, and J. Sweezy. *Trans. Am. Nucl. Soc.*, 87:273, 2002.

[7] W. Hauser and H. Feshbach. *Phys. Rev.*, 87:366, 1952.

[8] J. J. Griffin. *Phys. Rev. Lett.*, 17:478, 1966.

[9] A. V. Ignatyuk, K.K. Istekov, and G. N. Smirenkin. *Sov. J. Nucl. Phys.*, 29:450, 1979.

[10] A. V. Ignatyuk, J. L. Weil, S. Raman, and S. Kahane. *Phys. Rev. C*, 47:1504, 1993.

[11] N. Patronis, C. T. Papadopoulos, S. Galanopoulos, M. Kokkoris, G. Perdikakis, R. Vlastou, A. Lagoyannis, and S. Harrisopulos. *Phys. Rev. C*, 75:034607, 2007.

[12] M. Uhl and B. Strohmaier. Computer code for particle induced activation cross section and related quantities. Technical Report IRK-76/01, Vienna, 1976.

[13] M. Herman, R. Capote, B. Carlson, P. Oblozinsky, M. Sin, A. Trakov, and V. Zerkin. Empire-ii, nuclear reaction model code, version 2.19. Technical report, Vienna, 2005.

[14] O. Bersillon, F. Gunsing, E. Bauge, R. Jacqmin, and S. Leray, editors. *TALYS-1.0*, France, 2008. EDP Sciences.

[15] V. Avrigeanu, S. V. Chuvaev, R. Eichin, A. A. Filatenkov, R. A. Forrest, H. Freiesleben, M. Herman, A. J. Koning, and K. Seidel. *Nucl. Phys. A*, 765:1–28, 2006.

[16] M. Diakaki. Theoretical study of the $^{197}Au(n, 2n)$ reaction using the STAPRE-F code. Master's thesis, Department of Physics, School of Applied Sciences, National Technical University of Athens, 2010.

[17] W. Dilg, W. Schantl, H. Vonach, and M. Uhl. *Nucl. Phys. A*, 217:269, 1973.

[18] A. Gilbert and A.G.W Cameron. *Can. J. Phys.*, 43:1446, 1965.

[19] S. Sudar and S. M. Qaim. *Phys. Rev. C*, 73:034613, 2006.

[20] M. Al-Abyad, S. Sudar, M. N. H. Comsan, and S. M. Qaim. *Phys. Rev. C*, 73:064608, 2006.

[21] S. F. Mughaghab and C. Dunford. *Phys. Rev. Lett.*, 81:4083, 1998.

[22] M. B. Chadwick and P. G . Young. *Nuclear Science and Engineering*, 108:117–125, 1991.

[23] S. M. Mullins, G. D. Dracoulis, A. P. Byrne, T. R. McGoram, S. Bayer, W. A. Seale, and F. G. Kondev. *Phys. Lett. B*, 393:279, 1997.

[24] S. -C. Wu and H. Niu. *Nuclear Data Sheets*, 100:1, 2003.

[25] V.R. Vanin, N.L. Maidana, R.M. Castro, E. Achterberg, O.A. Capurro, and G.V. Marti. *Nuclear Data Sheets*, 108:2393, 2007.

[26] E. Achterberg, O. A. Capurro, G.V. Marti, V.R. Vanin, and R. M. Castro. *Nuclear Data Sheets*, 107:1–224, 2006.

[27] Yu. P. Gangrsky, N. N. Kolesnikov, V. G. Lukashik, and L. M. Melnikova. Isomeric ratios in reactions induced by gamma rays and fast neutrons in the isotopes of re, ir, and au. *Physics of Atomic Nuclei*, 67(7):1227–1232, 2004.

[28] E. Hagn and E. Zech. *Nucl. Phys. A*, 373:256–266, 1982.

[29] H. A. Tewes, A. A. Caretto, A. E. Miller, and D. R. Nethaway. Technical Report 6028, USA, 1960. Data retreived from EXFOR: www-nds.iaea.org/exfor.

[30] C. Phillis and O. Bersillon. Technical Report 4826, France, 1977. Data retreived from EXFOR: www-nds.iaea.org/exfor.

[31] J. F. Ziegler, J. P. Biersack, and U. Littmark. *The Stopping and Range of Ions in Solids*. Pergamon Press, New York, 1985.

[32] S. Sudar. A solution for the neutron spectrum unfolding problem without using input spectrum. Technical Report INDC(HUN)-026/L, Vienna, 1989.

[33] J. Bardeen, L. N. Cooper, and J. R. Schrieffer. Microscopic theory of superconductivity. *Phys. Rev.*, 106:162–164, 1957.

[34] H. A. Bethe. Nuclear physics b. nuclear dynamics, theoretical. *Reviews of Modern Physics*, 9(2):69–244, 1937.

[35] M. Avrigeanu, R. A. Forrest, F. L. Roman, and V. Avrigeanu. Technical report, Vancouver, BC, Canada, 1996.

[36] J. Raynal. Notes on ecis 94. Technical Report CEA-N-2772, CEA, Saclay, 1994.

[37] A. J. Koning and J. P. Delaroche. *Nucl. Phys.*, A713:231, 2003.

[38] T. Belgya, O. Bersillon, R. Capote, T. Fukahori, G. Zhighang, S. Goriely, M. Herman, A. V. Ignatyuk, S. Kailas, A. Koning, P. Oblozinsky, V. Plujko, and P. Young. Handbook for calculations of nuclear reaction data, ripl-2. Technical Report IAEA-TECDOC-1506, Vienna, 2006. Available online at http://www.nds.iaea.org/RIPL-2/.

[39] W. D. Myers and W. J. Swiatecki. *Ark. Fizik*, 36:343, 1967.

[40] P. Moller, J. R. Nix, W. D. Myers, and W. J. Swiatecki. *Atomic Data and Nuclear Data Tables*, 59:185–381, 1995.

[41] G. Audi, A. H. Wapstra, and C. Thibault. *Nucl. Phys. A*, 729:337, 2003.

[42] D. M. Brink. *Nucl. Phys.*, 4:215, 1957.

[43] P. Axel. *Phys. Rev.*, 126:671, 1962.

[44] H.M. Hofmann, J. Richert, J.W. Tepel, and H.A. Weidenmuller. *Ann. Phys.*, 90:403, 1975.

[45] L. McFadden and G. R. Satchler. *Nucl. Phys.*, 84:177, 1966.

[46] J. Kopecky and M. Uhl. *Phys. Rev. C*, 42:1941, 1990.

[47] A.J. Koning and M.C. Duijvestijn. A global pre-equilibrium analysis from 7 to 200 mev based on the optical model potential. *Nucl. Phys. A*, 744:15, 2004.

[48] S. Iwasaki, M. Sakuma, K. Sugiyama, and N. Odano. Cross section measurement for the neutron induced reactions on ni and au above 17 mev by activation technique. Technical Report JAERI-M-93-046, Japan, 1993.

[49] Lu Hanlin, Huang Jianzhou, Fan Peiguo, Cui Yunfeng, and Zhao Wenrong. Technical Report INDC(CPR)-16, Beijing, China, 1989. Data retreived from EXFOR: www-nds.iaea.org/exfor.

[50] B. P. Bayhurst, J. S. Gilmore, R. J. Prestwood, J. B. Wilhelmy, N. Jarmie, B. H. Erkkila, and R. A. Hardekopf. *Phys. Rev. C*, 12:451, 1975.

[51] S. I. Al-Quraishi, S. M. Grimes, T. N. Massey, and D.A. Resler. *Phys. Rev. C*, 67:015803, 2003.

[52] S. M. Qaim and A. Mushtaq. *Phys. Rev. C*, 38:645, 1988.

[53] A. J .Kreiner, M. Fenzl, S. Lunardi, and M.A. Mariscotti. Rotational structures in doubly odd ^{198} tl. *Nuclear Physics A*, 282:243–268, 1977.

[54] A. J. Kreiner. Particle-rotor model for doubly odd transitional nuclei of the tl-region. *Z. Physik A*, 288:373–381, 1978.

[55] E. F. Moore, M. P. Carpenter, Y. Liang, R. V. F. Janssens, I Ahmad, I. G. Bearden, P. J. Daly, M. W. Drigert, B. Formal, U. Garg, Z. W. Grabowski, H. L. Harrington, R. G. Henry, T. L. Khoo, T. Lauritsen, R. H. Mayer, D. Nisius, W. Reviol, and M. Sferrazza. *Phys. Rev. C*, 51:115, 1995.

[56] H. Hubel. *Prog. Part. Nucl. Phys.*, 38:89, 1997.

[57] N. Fotiades, S. Harissopulos, C. A. Kalfas, S. Kossionides, C. T. Papadopoulos, R. Vlastou, M. Serris, M. Meyer, N. Redon, R. Duffait, Y. Le Coz, L. Ducroux, F. Hannachi, I. Deloncle, B. Gall, M. G. Porquet, G. Schuck, F. Azaiez, J. Duprat, A. Korichi, J. F. Sharpey-Schafer, M. J. Joyce, C. W. Beausang, P. J. Dagnall, P. D. Forsyth, S. J. Gale, P. M. Jones, E. S. Paul, J. Simpson, R. M. Clark, K. Hauschild, and R. Wadsworth. *J. Phys. G: Nucl. Part. Phys.*, 21:911, 1995.

[58] N. Fotiades, S. Harissopulos, C. A. Kalfas, S. Kossionides, C. T. Papadopoulos, R. Vlastou, M. Serris, J. F. Sharpey-Schafer, M. J. Joyce, C. W. Beausang, P. J. Dagnall, P. D. Forsyth, S. J. Gale, P. M. Jones, E. S. Paul, P. J. Twin, J. Simpson, D. M. Cullen, P. Fallon, M. A. Riley, R. M. Clark, K. Hauschild, and R. Wadsworth. *Z. Phys.*, A:354, 1996.